JEM Journal of Experimental Medicine

ARTICLE

Functional vulnerability of liver macrophages to capsules defines virulence of blood-borne bacteria

Haoran An[1,2*], Chenyun Qian[1,2*], Yijia Huang[1*], Jing Li[1*], Xianbin Tian[1*], Jiaying Feng[1], Jiao Hu[1], Yujie Fang[1], Fangfang Jiao[1], Yuna Zeng[1], Xueting Huang[1,2], Xianbin Meng[3], Xue Liu[4], Xin Lin[1,2], Zhutian Zeng[5], Martin Guilliams[6,7], Alain Beschin[8,9], Yongwen Chen[10], Yuzhang Wu[10], Jing Wang[11], Marco Rinaldo Oggioni[12], John Leong[13], Jan-Willem Veening[4], Haiteng Deng[3], Rong Zhang[14], Hui Wang[15], Jiang Wu[16], Yan Cui[17], and Jing-Ren Zhang[1,2]

Many encapsulated bacteria use capsules to cause invasive diseases. However, it remains largely unknown how the capsules enhance bacterial virulence under in vivo infection conditions. Here we show that the capsules primarily target the liver to enhance bacterial survival at the onset of blood-borne infections. In a mouse sepsis model, the capsules enabled human pathogens *Streptococcus pneumoniae* and *Escherichia coli* to circumvent the recognition of liver-resident macrophage Kupffer cells (KCs) in a capsular serotype-dependent manner. In contrast to effective capture of acapsular bacteria by KCs, the encapsulated bacteria are partially (low-virulence types) or completely (high-virulence types) "untouchable" for KCs. We finally identified the asialoglycoprotein receptor (ASGR) as the first known capsule receptor on KCs to recognize the low-virulence serotype-7F and -14 pneumococcal capsules. Our data identify the molecular interplay between the capsules and KCs as a master controller of the fate and virulence of encapsulated bacteria, and suggest that the interplay is targetable for therapeutic control of septic infections.

Introduction

Sepsis is a common and often lethal syndrome with acute organ dysfunction (Rudd et al., 2020). The sepsis pathogenesis is a complex process, from overgrowth of invading pathogens in the blood circulation to dysregulated immune responses and collateral organ injuries (Munford and Suffredini, 2014). Encapsulated bacteria are the most common sepsis pathogens in humans and domestic animals (Wen and Zhang, 2015). Capsules are the outermost structures of many bacteria and certain fungi and are known to be essential for the in vivo survival and virulence of many bacterial pathogens. The importance of the capsule in bacterial virulence was elegantly used by Avery and his colleagues to demonstrate DNA as the genetic material (Avery et al., 1944). The significance of the capsules is also manifested by successful prevention of several human diseases caused by encapsulated bacteria using capsular polysaccharide (CPS)–based vaccines. Bacterial capsules have also been therapeutically targeted to treat bacterial infections with anti-capsule antibodies (Chang et al., 2002), phage-derived capsule depolymerases (Pertics et al., 2021), and capsule biosynthesis inhibiting small molecules (Arshad et al., 2016).

Virtually all known capsules are composed of repeating polysaccharide units, which are typically produced by single centralized *cps* loci (Moradali and Rehm, 2020; Whitfield et al., 2020). The structures of CPSs differ greatly between bacterial species. Many bacteria also produce intraspecies structural variants of CPSs by variations in the *cps* genes, which is the basis for conventional serotyping of bacterial strains (Whitfield et al., 2020). This is exemplified by identification of 100 and 83 capsular serotypes in *Streptococcus pneumoniae* and *Escherichia coli*, respectively (Ganaie et al., 2020; Wen and Zhang, 2015).

[1]Center for Infectious Disease Research, Department of Basic Medical Science, School of Medicine, Tsinghua University, Beijing, China; [2]Tsinghua-Peking Center for Life Sciences, Tsinghua University, Beijing, China; [3]School of Life Sciences, Tsinghua University, Beijing, China; [4]Department of Fundamental Microbiology, Faculty of Biology and Medicine, University of Lausanne, Lausanne, Switzerland; [5]School of Life Sciences, University of Science and Technology of China, Hefei, China; [6]Laboratory of Myeloid Cell Biology in Tissue Homeostasis and Regeneration, VIB Center for Inflammation Research, Ghent, Belgium; [7]Department of Biomedical Molecular Biology, Faculty of Science, Ghent University, Ghent, Belgium; [8]Myeloid Cell Immunology Lab, VIB Center for Inflammation Research, Brussels, Belgium; [9]Laboratory of Cellular and Molecular Immunology, Vrije University Brussel, Brussels, Belgium; [10]Institute of Immunology, Third Military Medical University, Chongqing, China; [11]Shanghai Institute of Immunology, School of Medicine, Shanghai Jiaotong University, Shanghai, China; [12]Department of Genetics and Genome Biology, University of Leicester, Leicester, UK; [13]Department of Molecular Biology and Microbiology, Tufts University School of Medicine, Boston, MA; [14]The Second Affiliated Hospital of Zhejiang University, Zhejiang University, Hangzhou, China; [15]Department of Clinical Laboratory, Peking University People's Hospital, Beijing, China; [16]Beijing Center for Disease Control and Prevention, Beijing, China; [17]Department of General Surgery, Strategic Support Force Medical Center, Beijing, China.

*H. An, C. Qian, Y. Huang, J. Li, and X. Tian contributed equally to this paper. Correspondence to Jing-Ren Zhang: zhanglab@tsinghua.edu.cn.

Structural variations in capsules are recognized as a mechanism for encapsulated bacteria to evade serotype-specific antibodies, which underlies the pneumococcal serotype replacement after vaccination with pneumococcal conjugate vaccines (Lo et al., 2019). Certain capsule types are more associated with the virulence traits of encapsulated bacteria than others in septic infections. This is manifested by the dominance of the low-numbered pneumococcal serotypes/serogroups in fatal pneumonia in pre-antibiotic era (e.g., serotypes 1–8; White, 1938). Similarly, K1 is the most frequently found capsule type of *E. coli* in neonatal meningitis patients (Robbins et al., 1974). However, it remains unclear how the capsule variants precisely impact bacterial virulence during septic infections.

Capsules have been designated as "slippery," or antiphagocytic, for decades because of the resistance of encapsulated bacteria to phagocytic killing of host defense (Comstock and Kasper, 2006; Wen and Zhang, 2015). Certain physical properties of the capsules (e.g., hyperviscosity and negative charge) hinder the recognition and binding of phagocytes to encapsulated cells (Brown and Gresham, 2012; Nahm and Katz, 2012; Taylor and Roberts, 2002). Capsules interfere with the complement-mediated opsonophagocytosis by masking the cell wall peptidoglycan and membrane-associated proteins (de Cordoba et al., 1983; Pangburn and Muller-Eberhard, 1978; Wilkinson et al., 1979). Certain bacteria evade host adaptive immunity by producing capsules structurally similar to host glycans, a phenomenon known as molecular mimicry (Finne, 1982; Troy, 1992; Wessels, 2006). A recent study shows that the capsule promotes intracellular survival and translocation of *S. pneumoniae* by enhancing bacterial resistance to oxidative killing (Brissac et al., 2021). However, it remains unknown what immune organs and cells are primarily targeted by bacterial capsules for immune evasion during septic infections.

In this study, we characterized the fates of blood-borne *S. pneumoniae* and *E. coli*, two common encapsulated sepsis pathogens, in a mouse sepsis model. The data uncovered the liver and its resident macrophage Kupffer cells (KCs) as the major organ and cells targeted by encapsulated bacteria to circumvent the most potent antibacterial machinery of the mammalian hosts against blood-borne microbes. Using isogenic bacteria producing different types of capsules, we further stratified the disease potential of selected capsule types of *S. pneumoniae* and *E. coli* into low- and high-virulence categories (LV and HV, respectively). The virulence phenotypes of individual capsule types were found to be predominantly determined by the natures of receptor–ligand interactions between the CPSs and KCs during the early phase of septic infections.

Results

Capsular serotypes define pneumococcal virulence

Previous studies have documented significant differences in virulence among pneumococcal strains/serotypes (Briles et al., 1992; Sjostrom et al., 2006; White, 1938). To understand the molecular basis of this heterogeneity, we first compared the virulence levels of 144 encapsulated strains representing 34 serotypes in a murine septic infection model (Fig. 1 A). This revealed remarkable differences in virulence as characterized by mortality rate in the 7-d observation period. We empirically used 50% mortality as a cutoff value to divide these strains into the categories of HV (48 strains) and LV (96 strains; Fig. 1 B and Table S1). The HV and LV mortality phenotypes were also reflected by bacteremia level (Fig. 1, B and C) and survival time (Fig. 1 D). The mice infected with the HV strains typically progressed to more severe bacteremia at 12 and 24 h, as high as 10^9 CFU/ml blood. In contrast, infection with the LV strains displayed relatively low levels of bacteremia. Accordingly, the mice infected with the HV strains showed much shorter survival time than LV counterparts. Further investigation with selected HV and LV strains, as well as the acapsular mutant R6, revealed remarkably large margins in virulence among pneumococcal strains. The HV strain TIGR4 (type 4) and TH870 (type 6A) were still fully virulent at an extremely low inoculum of 100 CFU (Fig. S1 A); the LV strains ST556 (type 19F) and TH2919 (type 6B) became fully virulent when infection dose was increased to 10^8 CFU (Fig. S1 B). However, R6 remained avirulent even at the highest infection dose (Fig. S1 B). This result showed a wide range of disease potential for encapsulated pneumococci.

Further analysis revealed a clear correlation between virulence and capsular serotype (Fig. 1 E). While all tested strains of eight serotypes fell into the HV category (1, 2, 3, 4, 5, 8, 22F, and 38), those of 23 other serotypes uniformly showed the LV phenotype. Only the strains of serotypes 6A, 6B, and 6C exhibited both LV and HV phenotypes. To ascertain this relationship, we constructed isogenic strains expressing different capsular serotypes by genetic replacement of the *cps* gene cluster (Fig. 2 A). Although the *cps* deletion mutant of the HV strain TH870 (serotype 6A) became avirulent in the murine sepsis model, complementation with the heterologous *cps* gene clusters of serotype 1, 2, 3, 4, 5, 6A, or 8 conferred the HV virulence phenotype to the mutant with 100% mortality and persistent bacteremia (Fig. 2 B, red lines). In sharp contrast, the counterpart carrying the *cps* locus of serotype 6B, 7F, 9V, 14, 18C, 19F, 19A, or 23F completely abolished the original HV phenotype of TH870. All of the mice infected with these strains survived with barely detectable bacteremia (Fig. 2 B, green lines). The role of capsule serotypes in shaping pneumococcal virulence was also demonstrated in capsule-switched derivatives of strains TH2919 (serotype 6B; Fig. 2 C), TH197 (serotype 6A; Fig. S1 C), and TH2912 (serotype 14; Fig. S1 D). One exception of this causal relationship between capsule serotype and virulence phenotype was observed with a derivative of serotype 3 strain TH2891. Expressing the serotype 6A *cps* genes (an HV capsule type) in TH2891 resulted in an unexpected LV phenotype (Fig. S1 E). This outlying effect may be caused by functional mismatch between the *cps* genes and the genetic background of the recipient strains, as reported previously (Wen et al., 2016).

Finally, we characterized the virulence of isogenic type 6A and 6B strains that differed only in a single nucleotide at position 584 of *wciP*, encoding the rhamnosyl transferase for biosynthesis of the serogroup 6 capsules (Mavroidi et al., 2004). The type 6A and 6B capsules consist of identical tetrasaccharide repeating units with only a different linkage between the rhamnose and ribitol-5-phosphate residues (α1–3 in 6A, α1–4 in 6B; Han et al.,

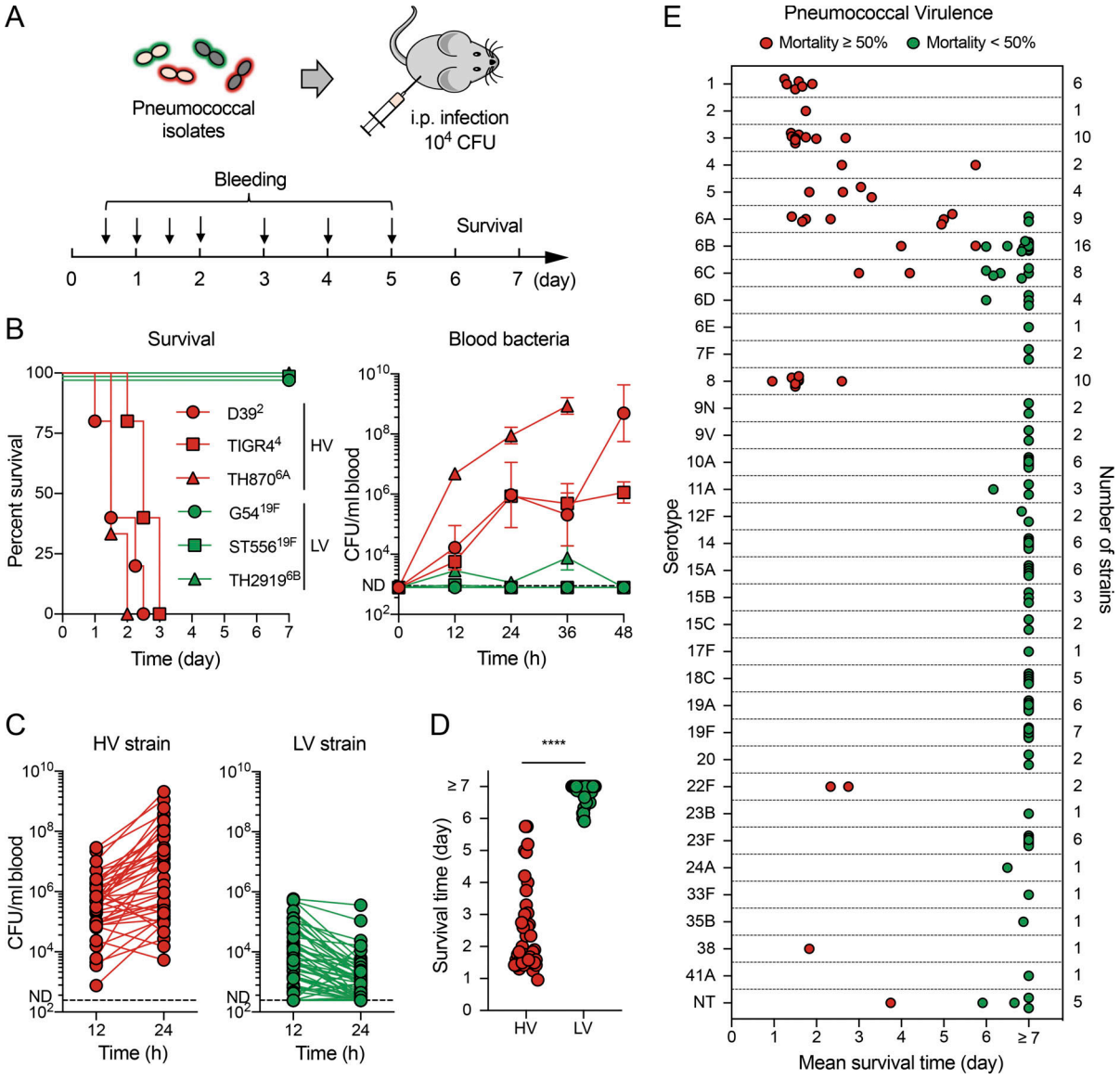

Figure 1. **Strain-to-strain variations in the virulence level of *S. pneumoniae*. (A)** Schematic workflow of systemic assessment of the virulence levels of pneumococcal isolates in murine sepsis model. **(B)** Survival (left) and bacteremia (right) levels of CD1 mice infected i.p. with 10^4 CFU of representative HV (red line) and LV (green line) pneumococcal isolates. Serotype of each strain is denoted with superscript characters. *n* = 5–6. ND, not detected. **(C)** Bacteremia kinetics of the 48 HV (left) and 96 LV (right) strains 12 and 24 h after infection as in B. Each dot represents the mean value of five to nine mice for one strain. Lined dots indicate the values for the same strain at two time points. **(D)** Mean survival time of the mice infected with the same HV and LV strains as in B. Each dot represents the mean value for one strain. **(E)** Correlation between pneumococcal serotypes and mean survival times of mice infected as in B. The number of strains tested for each serotype is indicated at the right. All data were pooled from two independent experiments. Unpaired *t* test (D), ****, P < 0.0001.

2012; Fig. 2 D). A G_{584} (serine$_{195}$ in 6A)-to-A_{584} (asparagine$_{195}$ in 6B) polymorphism in *wciP* defines the rhamnosyl-ribitol-5-P linkage and thereby the structural difference between the two capsules (Mavroidi et al., 2004). While a G-to-A mutation at position 584 of *wciP* in TH870^{6A} resulted in an LV phenotype, an opposite (A-to-G) mutation in the corresponding site of TH2919^{6B} converted the otherwise LV strain to HV (Fig. 2 E).

Because invasive pneumococcal diseases are naturally developed from pneumonia (Musher and Thorner, 2014), we investigated the impact of capsule types on pneumococcal virulence phenotypes in respiratory infection model. In line with their virulence phenotypes in septic infection, the selected HV (3, 6A, and 8) and LV (14, 19F, and 23F) serotypes displayed the same patterns of virulence traits in mice infected by intratracheal (i.t.) inoculation. Whereas airway infection of serotypes 3, 6A, and 8 led to 100% mortality (Fig. 2 F), with gradually worsening bacteremia as early as 12 h after infection (Fig. 2 G), all of the mice infected with serotypes 14, 19F, and 23F survived with no or marginal bacteremia (Fig. 2, F and G). Together with the clinical surveys (Brueggemann et al., 2004; Sjostrom et al., 2006; Weinberger et al., 2010; White, 1938), these data demonstrate a decisive role of capsule structures in defining pneumococcal virulence.

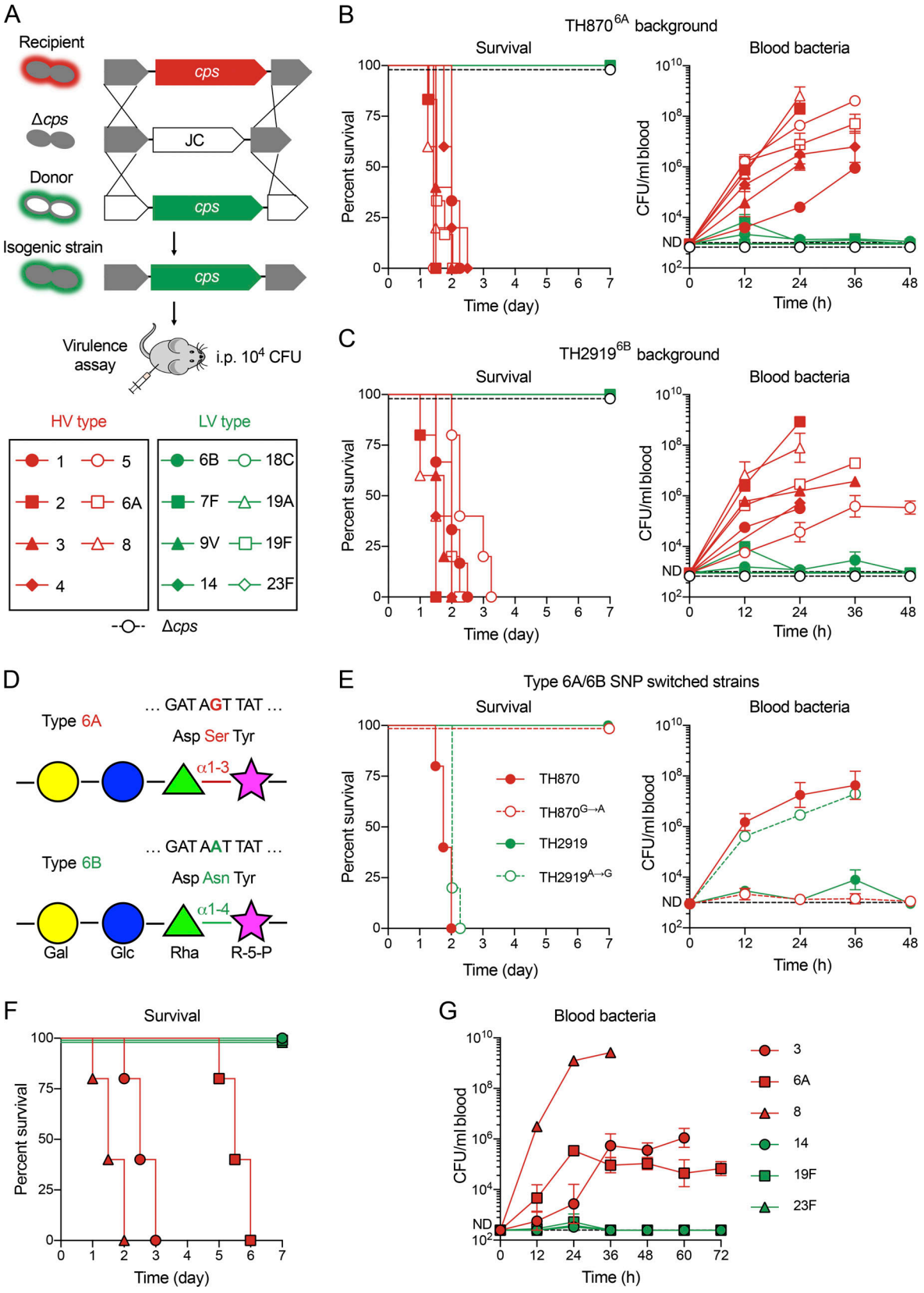

Figure 2. **Causal relationship between capsule types and virulence phenotypes. (A)** Schematic illustration of the capsule-switching scheme. The *cps* gene clusters of target (recipient) strains were first replaced with JC to produce unencapsulated mutants, which were then transformed with the *cps* gene amplicons of donor strains to yield capsule replacement strains. Selected HV (red symbols) and LV (green symbols) serotypes are indicated below. **(B)** The levels of survival (left) and bacteremia (right) of CD1 mice infected i.p. with 10^4 CFU of the isogenic capsule variants generated in serotype 6A strain TH870^{6A}. *n* = 5–6.

(C) Same as B except for using the isogenic variants of serotype 6B strain TH2919^{6B}. *n* = 5–6. **(D)** The differences in the sequence of *wciP* and CPS repeating unit between serotypes 6A and 6B. The polymorphic nucleotide and corresponding amino acid sequences of *wciP* and linkage between rhamnose and ribitol-5-phosphate in serotypes 6A and 6B are depicted. Glc, glucose; Gal, galactose; Rha, rhamnose; R-5-P, ribitol-5-phosphate. **(E)** Same as B except for using the isogenic strains with reciprocal single nucleotide polymorphism (SNP) switches in the TH870^{6A} and TH2919^{6B} backgrounds. *n* = 5. **(F and G)** The levels of survival (F) and bacteremia (G) of CD1 mice after i.t. infection with 10^7 CFU of the isogenic strains. *n* = 5. All data were pooled from two independent experiments.

HV capsules enable pneumococci to bypass hepatic capture

To determine how the capsules enhance bacterial survival during septic infection, we compared the bacterial dynamics in the blood and major organs in mice after i.v. infection with isogenic derivatives of encapsulated TH870 (serotype 6A; Fig. 3 A). In keeping with the importance of the capsule in pneumococcal virulence, infection with TH870 (WT) led to 100% mortality, but all of the mice infected with acapsular mutant (Δ*cps*) survived (Fig. S2 A). Accordingly, the Δ*cps* mutant became undetectable in the blood circulation within the first 30 min, whereas the parental bacteria were abundantly present (Fig. 3 B). To characterize the fates of the Δ*cps* mutants disappearing from the circulation, we determined bacterial distribution in five major organs at various time points after i.v. inoculation. The vast majority of the Δ*cps* mutants (77.3%) were found to be already trapped in the liver as early as 5 min, whereas only a small fraction of the encapsulated counterparts was detected in the liver (21.9%; Fig. 3 C). At that time, the liver trapped 4.7-fold more Δ*cps* mutants than the WT strain (Fig. 3 D). The spleen housed the second highest proportions of bacteria for both TH870 (14.4%) and its acapsular mutant (15.3%); heart, kidney, and lung contained only residual levels of bacteria (Fig. 3 C). These data reveal that the capsule is extremely important for bacterial survival in the bloodstream by blocking hepatic capture at the very beginning of septic infection.

To define how the capsule type shapes pneumococcal virulence, we characterized the bacteremia kinetics of isogenic LV (serotypes 14, 19F, and 23F) and HV (serotypes 3, 6A, and 8) derivatives of TH870. The virulence phenotypes of isogenic capsule serotype switched strains obtained by i.v. inoculation fully recapitulated those by the i.p. infection route (Fig. 2). All of the mice infected with the HV counterparts succumbed to challenge, whereas those with the LV strains survived (Fig. S2 B). Accordingly, the HV counterparts were temporally reduced in the first 12 h, but rebounded later. In contrast, the LV serotypes were virtually undetectable in the bloodstream in the first 12 h and remained undetectable ever since (Fig. S2 C). Similar to the rapid clearance of the acapsular mutant (Fig. 3B), the three LV serotypes became barely detectable in the bloodstream in the first 10–20 min after i.v. infection (Fig. 3 E). By comparison, the HV counterparts were abundantly present at 30 min. 5 min after i.v. inoculation, the vast majority of the LV pneumococci were found in the liver (type 14, 98.7%; 19F, 81.5%; and 23F, 74.8%); whereas the majority of the HV bacteria were still circulating in the bloodstream with only small fractions in the liver (type 3, 11.2%; 6A, 21.9%; and 8, 16.4%; Fig. 3, F and G). This serotype-dependent sequestration of pneumococci in the liver still operated at 10 and 30 min (Fig. S2 D). Besides the liver, the spleen, but not the heart, kidneys, or lungs, contained small fractions of bacteria for serotypes 3 (10.5%), 6A (12.4%), 8 (11.6%), 19F (13.1%), and 23F (17.2%; Fig. 3 F). This result indicates that the capsule serotype–dependent virulence phenotypes in septic infection are decided by differential trapping of blood-borne bacteria in the liver at a very early phase.

To determine the fate of the LV pneumococci captured in the liver, we compared the total viable bacteria of six representative serotypes at various time points after i.v. inoculation. The results showed gradual but effective elimination of the LV serotypes in the first 30 min. Despite rapid deposition of the LV bacteria in the liver, the total bacteria of serotypes 14, 19F, and 23F recovered from the blood and five organs were similar to the inocula for all isogenic strains at 5 min (Fig. 3 H), indicating that the bacteria captured in the liver were not immediately killed. However, the CFU in the livers and other organs of mice infected by the LV bacteria were significantly diminished at later time points (Fig. 3, I and J). In particular, at 30 min, only minor fractions of the originally inoculated serotype-14 (4.7%), -19F (12.8%), and -23F (12.3%) bacteria were detected (Fig. 3 J). In sharp contrast, high proportions of the inocula were still present in the mice infected by serotypes 3 (91.2%), 6A (66.8%), and 8 (62.9%) at 30 min (Fig. 3 J). These data demonstrate that the liver effectively captures and kills the LV encapsulated pneumococci but not HV counterparts during the early phase of septic infection.

Because the spleen was the organ with the second-highest proportions of pneumococci (Fig. 3, C and F), we evaluated the contribution of the organ to the early clearance of blood-borne bacteria using splenectomized (SPX) mice. Surgical removal of the spleen did not impair the clearance of isogenic serotype-8 (HV) and -14 (LV) pneumococci by the liver in the first 30 min of infection (Fig. 3 K). In fact, the liver of the SPX mice contained virtually all viable bacteria of TH870^{14} at 30 min, which appeared to be a compensatory response of the liver in the absence of the spleen. The asplenic mice showed a relatively higher level of serotype-8 pneumococci in the circulation and liver than sham-operated mice (Fig. 3 L). This observation indicates that the spleen is able to trap a low level of HV pneumococci that are poorly caught by the liver, which agrees with previous findings that the spleen is important for combating *S. pneumoniae* and other encapsulated bacteria (Deniset et al., 2017; Theilacker et al., 2016). Together, these data demonstrate that the liver but not spleen is the dominant organ responsible for rapid elimination of LV serotypes at the onset of septic infection.

We finally assessed the role of the liver in the clearance of blood-borne bacteria derived from pneumococcal pneumonia by i.t. instillation of 10^7 CFU isogenic HV (type 8) or LV (type 14) pneumococci. Both the strains caused severe bacterial burden in the lungs at 12 h (Fig. 3 M). While the mice infected with

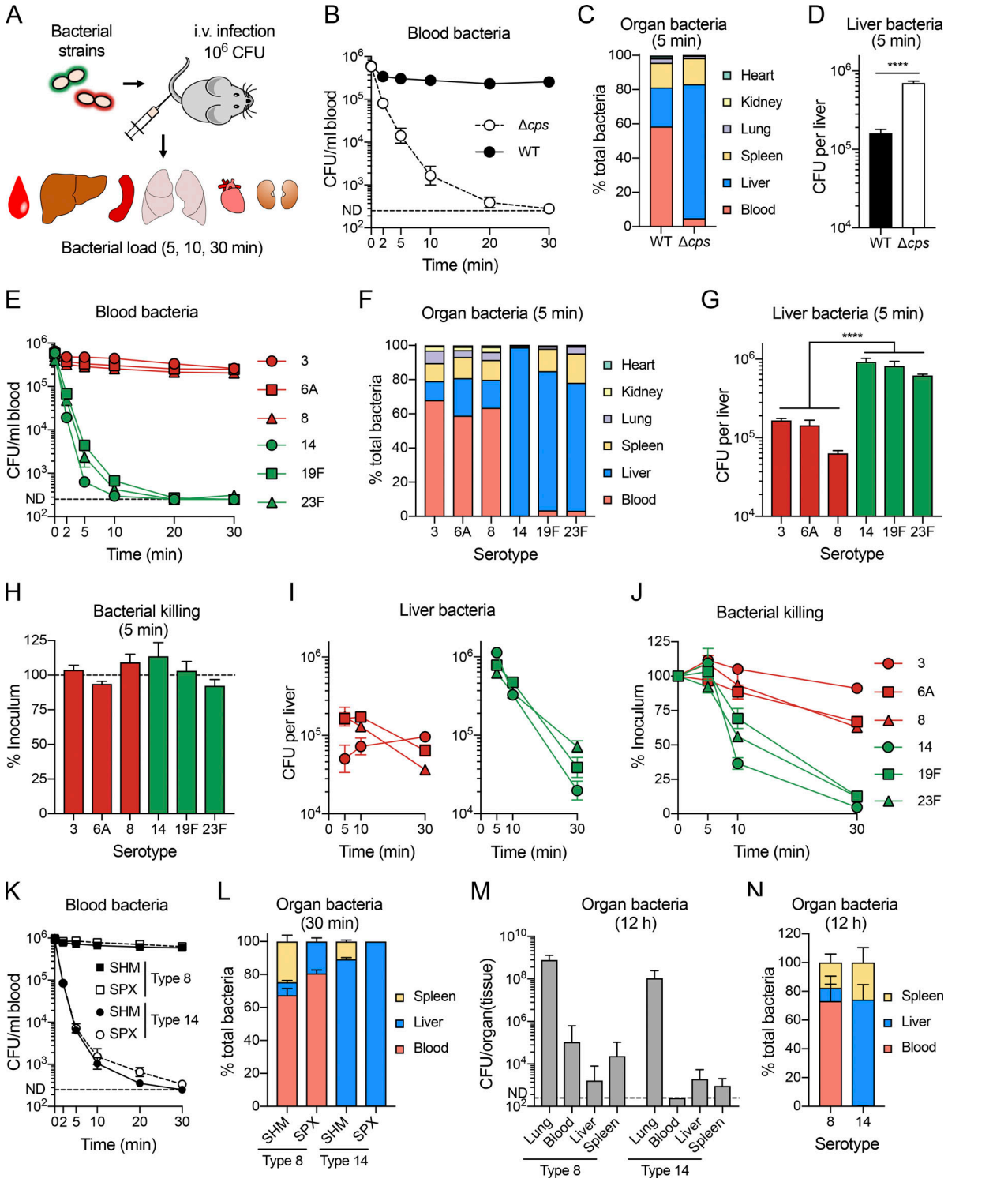

Figure 3. **Impact of pneumococcal capsule on hepatic trapping. (A)** Illustration of experimental detection of bacteria localization in CD1 mice after i.v. infection with 10^6 CFU of isogenic TH870 derivatives. **(B)** Bacteremia kinetics of WT or acapsular (Δ*cps*) strain in the first 30 min of infection. *n* = 5. **(C)** Proportional distribution of WT and Δ*cps* in the blood and organs at 5 min after infection. *n* = 3. **(D)** Bacterial load in the liver at 5 min. *n* = 3. **(E)** Bacteremia kinetics of HV (red) and LV (green) serotypes as in B. *n* = 5–6. **(F)** Proportional distribution of HV (red) and LV (blue) serotypes in the blood and organs at 5 min. *n* = 3. **(G)** Bacterial load in the liver at 5 min as in F. **(H)** Viable isogenic HV and LV pneumococci detected in the blood and five major organs of mice at 5 min after infection. *n* = 3. **(I)** Kinetics of viable HV (left) and LV (right) pneumococci in the liver of mice during the first 30 min of infection. *n* = 3–9. **(J)** Kinetics of viable pneumococci detected in the blood and organs in the first 30 min. The CFU values are presented as ratios of the corresponding inoculum sizes. *n* = 3–9. **(K and L)** Bacteremia kinetics (K) and proportional distribution (L) of serotype-8 and -14 pneumococci in SPX and SHM mice in the first 30 min of infection. *n* = 3–6. **(M and N)** Bacterial load (M) and proportional distribution (N) of serotype-8 and -14 pneumococci 12 h after i.t. instillation with 10^7 CFU. *n* = 3–6. Data were from one experiment (C, D, and F–H) or pooled from two independent experiments (B, E, and I–N). Unpaired *t* test (D), ordinary one-way ANOVA with Dunnett's multiple comparisons test (G), ****, P < 0.0001.

serotype-8 pneumococci showed bacteria in the blood, liver, and spleen, bacteria were detected in the liver and spleen, but not in blood, of mice i.t. infected with serotype-14 bacteria. The disseminating serotype-8 bacteria were predominantly found in the blood circulation, with relatively small fractions in the liver and spleen. In sharp contrast, the vast majority of disseminating serotype-14 pneumococci were trapped in the liver, making the blood sterile (Fig. 3 N). This finding indicates that the liver captures pneumococci disseminating from the lung to the blood circulation in the same serotype-dependent manner as shown in the septic infection model.

LV serotypes evade hepatic capture at high infection doses

It is intriguing that a number of LV capsule types identified in mouse models are included in the current pneumococcal vaccines, since they are associated with invasive infections of humans, such as 6B, 9V, 14, 18C, 19A, 19F, and 23F (Feldman and Anderson, 2020). We reasoned that these LV serotypes are superior to acapsular strains in the escape of hepatic capture at relatively high levels of bacteremia. We thus compared the clearance kinetics between isogenic serotype 14 and acapsular derivatives of TH870 in mice infected i.v. with 10^8 CFU. This trial showed that the encapsulated LV pneumococci are much more capable of surviving in the blood circulation and evading hepatic capture than the acapsular mutant. While the Δ*cps* strain was almost fully cleared from the circulation in the first 30 min, TH870[14] was abundantly present in the bloodstream (144-fold higher than Δ*cps*; Fig. 4 A). In keeping with the relatively poorer hepatic capture of TH870[14] from the circulation (Fig. 4 B), 20% of its inoculum was still detectable in the host at 30 min, compared with only 5% of the Δ*cps* counterpart (Fig. 4 C). This observation is in line with 50% lethality of asialoglycoprotein receptor (ASGR) deficient ($ASGR1^{-/-}$) mice when this dose of TH870[14] was used (see Fig. 8). This result indicates that the encapsulated LV capsules are able to evade hepatic capture when invading bacteria reach certain levels in the circulation.

To assess the functional range of the capsule-mediated immune evasion, we compared the clearance rates of isogenic serotype-3 and -14 strains from the circulation of mice at various infection doses. The LV pneumococci were fully eradicated from the circulation within 30 min at infection doses as high as 10^7 CFU (Fig. 4 D). In contrast, serotype-3 pneumococci were stably circulated at all the infection doses (Fig. 4 E). In particular, the HV bacteria were still detectable in the bloodstream even with an inoculum of 10^3 CFU. The striking difference between the LV and HV capsule types in immune evasion is also reflected by their 50% clearance times (CT_{50}, the time for clearing 50% inoculum from the bloodstream; Fig. 4 F). The intrinsic differences among capsule types in escaping hepatic capture allowed us to rank 15 selected serotypes based on CT_{50} levels of isogenic strains. This analysis places serotypes 3 and 14 at the extreme ends of this immune evasion spectrum, with CT_{50} values of 0.4 and 24.3 min, respectively (Fig. 4 G). Together, these results demonstrate that the serotype-specific potency in evading hepatic capture defines the disease potential of pneumococcal capsule variants in septic infection.

Phagocytic function of KC is differentially impaired by pneumococcal capsules

To identify the immune cells in the liver whose function was compromised by the capsules, we assessed the contribution of major professional phagocytes to hepatic clearance of acapsular Δ*cps* by selective depletion (Fig. 5 A; and Fig. S2, E and F). Although neutrophils are reported to be important for eliminating blood-borne microbes (Derby and Rogers, 1961; Munford and Suffredini, 2014; Rogers, 1956), depleting neutrophils with the 1A8 antibody did not affect the clearance rate (Fig. 5, B and C), hepatic capture (Fig. 5 D), and bacterial killing (Fig. 5 E) of Δ*cps* in the first 30 min. Treatment with the Gr1 antibody (depleting monocytes and neutrophils) also had little impact on the Δ*cps* clearance (Fig. 5, B–E). In contrast, exhausting liver-resident macrophage KCs led to a dramatic reduction in the clearance of acapsular pneumococci. Treating the *Clec4f*-DTR mice (Scott et al., 2016) with diphtheria toxin (DT) increased bacteremia levels by 42.9-, 72.8-, 599.2-, and 215.4-fold at 5, 10, 20, and 30 min (Fig. 5 B). CT_{50} was elongated from 0.53 min in control mice to 3.1 min in DT-treated mice (Fig. 5 C). The KC-depleted mice were severely impaired in shuttling acapsular pneumococci from the bloodstream to the liver (Fig. 5 D). While the livers of control mice carried 70.6% of the inoculum 10 min after infection, this value was reduced to only 9.9% in DT-treated mice. Depletion of KCs also led to significant impairment of bacterial killing: >30% of the inoculum was detected in the host at 30 min compared with <10% in the control (Fig. 5 E). The importance of KCs in the capture of acapsular bacteria was also demonstrated by intravital microscopy (IVM) imaging of liver sinusoids. Consistent with rapid capture of acapsular bacteria in the liver (Fig. 3 E), the Δ*cps* mutants were abundantly docked on KCs immediately after i.v. inoculation, while the parental bacteria mostly moved through the sinusoid vasculatures (Fig. 5 F and Video 1). The Δ*cps* bacteria were no longer detained in the liver sinusoids of the DT-treated mice owing to the lack of KCs (Fig. 5 G and Video 2). These results strongly suggest that the liver-resident macrophage KCs are responsible for effective capture and killing of the unencapsulated bacteria.

We further investigated the impact of different capsular types on the interplay of pneumococci and liver KCs. As visualized by IVM, the isogenic LV strains (types 14, 19F, and 23F) were rapidly and abundantly docked on KCs after i.v. inoculation, while the HV counterparts (types 3, 6A, and 8) mostly moved through the sinusoid vasculatures (Fig. 6 A; Fig. S2 G; and Video 3). As exemplified with serotype 14 pneumococci, each KC could bind as many as 20 LV bacterial cells compared with ≤1 HV bacterium 20 min after inoculation (Fig. 6 A, left panel). Not surprisingly, the DT-treated *Clec4f*-DTR mice were severely impaired in shuttling the LV pneumococci of serotypes 14, 19F, and 23F from the bloodstream to the liver (Fig. 6, B–D; Fig. S2 H; and Video 4). Selective detection of intramacrophage bacteria by pHrodo labeling revealed that 29.5% of the type 14 pneumococci were engulfed by KCs as early as 20 min (Fig. 6 E), indicating the bactericidal role of KCs by phagocytic killing. Functionally, the absence of KCs made the host highly susceptible to septic infection with LV type 14 pneumococci, as reflected by sustained bacteremia (Fig. S2 I) and 100% mortality of the KC-depleted

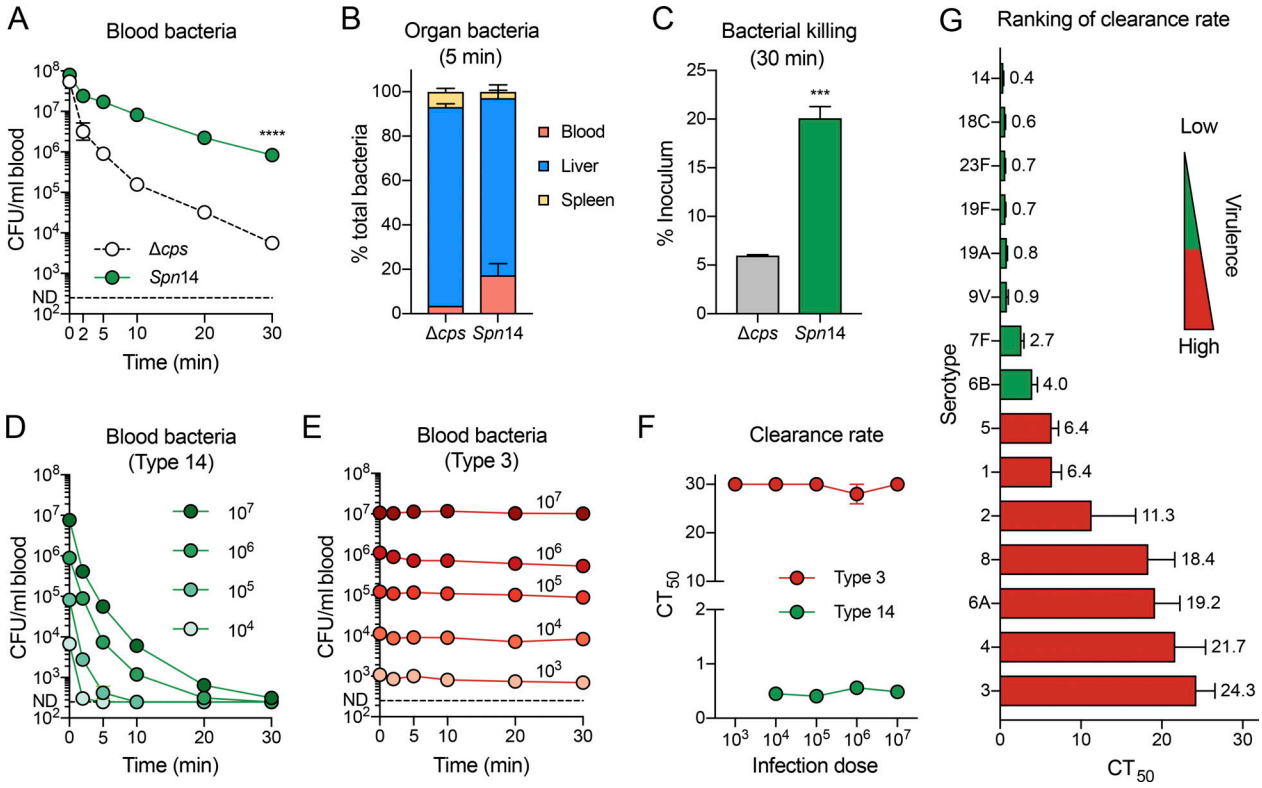

Figure 4. **Impact of capsular types on pneumococcal clearance rate in the bloodstream. (A–C)** Bacteremia kinetics in the first 30 min (A), proportional distribution at 5 min (B), and bacterial viability at 30 min (C) after i.v. infection of CD1 mice with 10^8 CFU of acapular (Δ*cps*) and serotype-14 derivatives of TH870 (*Spn*14). *n* = 3. **(D–F)** Bacteria in the bloodstream of CD1 mice infected i.v. with 10^3–10^7 CFU in the first 30 min. Data are presented as bacteremia kinetics of serotypes 14 (D) and 3 (E) or CT_{50} (F). *n* = 3–6. **(G)** Ranking of 15 pneumococcal serotypes based on the CT_{50} values of isogenic capsule-switched derivatives of TH870 in CD1 mice infected i.v. with 10^6 CFU. *n* = 5–6. CT_{50} was calculated by nonlinear regression of bacteremia data, which is presented as 30 min when >50 of the inoculum was still detectable in the circulation. Data were from one experiment (A–C) or pooled from two independent experiments (D–G). Two-way ANOVA with Tukey's multiple comparisons test (A), unpaired *t* test (C), ***, P < 0.001, ****, P < 0.0001.

mice (Fig. 6 F), akin to the HV-bacterial infection in normal mice (Fig. S2, B and C). These results thus demonstrate a pivotal role of KC-mediated early clearance for the host defense against septic infection of the LV capsule types.

Finally, we verified binding interactions between primary KCs and pneumococci. The freshly isolated KCs from mouse liver showed significant adherence to isogenic LV pneumococci of serotypes 14, 19F, and 23F but were poorly adherent to the HV counterparts of serotypes 3, 6A, and 8, even with opsonization by normal mouse serum (Fig. 6 G). In a similar manner, the primary human KCs caught 20–30% of the LV pneumococci in the ex vivo system, whereas binding to HV pneumococci was significantly lower (Fig. S2 J). Together, these experiments demonstrate that KCs are primarily responsible for the capture of LV pneumococci in the liver during septic infection; in contrast, the HV capsule variants inherently bypass the surveillance by KCs.

LV capsules are the ligands for KC recognition

Whereas KCs are known to express an array of pattern recognition receptors (PRRs) for clearance of blood-borne pathogens (Jenne and Kubes, 2013), no PRRs on KCs are known to recognize bacterial capsules. Rapid clearance of encapsulated LV pneumococci by KCs suggested that the CPSs of the LV pneumococci are potential ligands for host receptors on KCs. We tested this possibility by pretreatment with free CPSs of three representative LV serotypes (types 14, 19F, and 23F) before bacterial inoculation (Fig. 7 A). Intravenous injection of type 14 CPS (CPS14) immediately before inoculation of TH870[14] expressing a homologous serotype 14 capsule resulted in dose-dependent reduction of bacterial clearance (Fig. 7 B, left panel). For instance, CT_{50} was elongated to 4.3 min in the mice treated with 400 µg of CPS14 from 0.35 min in the control (Fig. 7 B, right panel). The delayed clearance accompanied a dose-dependent decline in hepatic capture (Fig. 7 C). Ultimately, pretreatment with higher doses of CPS14 (e.g., 400 µg) made 56.1% of the inoculum viable at 30 min compared with only 2% in the control (Fig. 7 D). Significant inhibition against clearance of homologous serotypes was also achieved with CPS19F and CPS23F (Fig. 7 E; and Fig. S3, A and B). The blocking effect of the LV CPSs also accompanied significant reduction in KC-mediated bacterial capture in the liver sinusoids (Fig. 7 F and Video 5). However, similar treatment with CPSs of HV serotypes 3, 6A, and 8 did not yield any impact on the clearance of the homologous pneumococci (Fig. 7 E; and Fig. S3, C and D). The poor recognition of HV CPSs by KCs was further manifested by the observation that pretreatment of mice with different amounts of purified CPS3 did not affect the clearance of a sublethal dose of serotype-3 pneumococci (10^5

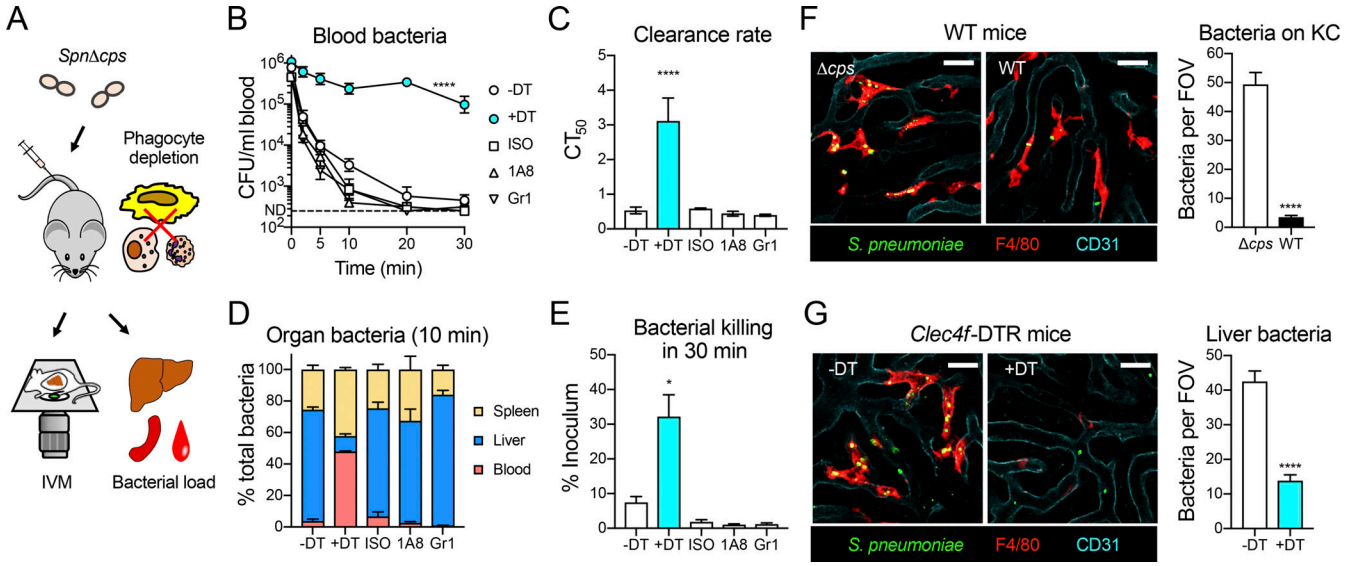

Figure 5. **Capture of acapsular pneumococci by KCs. (A)** Schematic depiction of experimental design to assess the contribution of major phagocytes to the hepatic clearance of acapsular bacteria. **(B–E)** Bacteremia kinetics (B), clearance rates during the first 30 min (C), proportional distribution at 10 min (D), and bacterial killing in 30 min (E) after i.v. infection of phagocyte-depleted mice with 10^6 CFU of Δ*cps*. *Clec4f*-DTR mice were treated with (+DT) or without (–DT) 10 ng/g body weight of DT, and WT mice were treated with 500 µg of each antibody 24 h before i.v. infection. *n* = 3–5. **(F and G)** IVM detection of bacterium-binding KCs. Representative IVM images exemplify the KCs (red), pneumococci (green), and sinusoid endothelial cells (cyan) in the liver sinusoids of WT (F) and *Clec4f*-DTR (G) mice 10 min after i.v. infection with 5 × 10^7 CFU of pneumococcal strains. *n* = 3. Five to 10 random fields of IVM images were quantified as bacteria per field of view (FOV) and presented at the right of the images. Scale bar, 20 µm. All mice were used on a C57BL/6 background. Data were representative results (F and G) or pooled (B–E) from two independent experiments. Two-way ANOVA with Tukey's multiple comparisons test (B), ordinary one-way ANOVA with Tukey's multiple comparisons test (C and E), *, P < 0.05, ****, P < 0.0001.

CFU; Fig. S3, E and F). This information strongly suggests that KCs capture the LV but not HV pneumococci through molecular recognition of CPS structures.

We next assessed the ligand specificity in KC's recognition of the LV capsules by testing the impact of free CPSs on the clearance of heterologous serotypes. The clearance of TH870[14] was blocked by pretreatment with CPS14 only, but not with any CPS of seven heterologous LV serotypes (6B, 7F, 9V, 18C, 19A, 19F, and 23F; Fig. 7 G and Fig. S3 G). The clearance of isogenic serotype 19F (Fig. 7 H and Fig. S3 H) and 23F (Fig. 7 I and Fig. S3 I) pneumococci was similarly attenuated in a serotype-specific manner by CPS19F and CPS23F, respectively, but not by CPSs of heterologous serotypes. The serotype-specific blocking indicates that the LV capsules are recognized by specific receptors on KCs. The null blocking of the HV CPSs further supports the concept that the HV capsules are poorly recognized by KCs.

The role of the complement system in the clearance of LV serotypes was investigated using mice lacking complement protein C3 or complement receptor of Ig superfamily (CRIg). Activated C3 promotes opsonophagocytic killing of pneumococci (Hyams et al., 2011), and CRIg is the major complement receptor on KCs, with significant contribution to bacterial capture (Helmy et al., 2006). As shown in Fig. 7 J, the clearance of serotype-19F and -23F pneumococci was dramatically impaired in the C3-deficient mice, but serotype-14 bacteria were still effectively eliminated from the blood of the $C3^{-/-}$ mice, indicating that C3 is necessary for KC recognition of serotype-19F and -23F but not -14 pneumococci. In keeping with this finding, $CRIg^{-/-}$ mice showed significantly slower clearance of serotype-19F and -23F pneumococci, particularly at 10 min (Fig. 7 K). In contrast, serotype-14 bacteria were removed from the bloodstream at a similar pace in both WT and $CRIg^{-/-}$ mice. These results show that the complement system is involved in the KC capture of certain but not all LV pneumococcal serotypes.

ASGR on KCs recognizes serotype-7F and -14 pneumococcal capsules

Because hepatic capture of serotype-14 pneumococci is independent of the complement system (Fig. 7 J), we sought to identify the CPS14 receptors on KCs by affinity pulldown of proteins from murine nonparenchymal cells (NPCs) with CPS14-coated beads (Fig. 8 A). The CPS8-conjugated beads were used as negative controls because this serotype is poorly captured by KCs (Fig. 6 A). Mass spectrometry analysis identified 81 membrane-associated proteins that were significantly enriched by the CPS14-conjugated beads (Fig. 8 B and Table S2).

Expression of the top hits in Chinese hamster ovary (CHO) cells resulted in significantly enhanced adhesion to TH870[14] only with the murine ASGR1 construct. The ASGR1-expressing cells captured 45.5% of TH870[14], but transfection with the other candidates (e.g., ASGR2, CD36, C1qbp, and endoglin) did not yield significant impact (Fig. 8 C). ASGR1 and ASGR2 are two integral subunits of ASGR, a C-type lectin that is uniquely expressed in the liver (Hoober, 2020). ASGR mediates endocytosis and lysosomal degradation of desialylated glycoproteins and platelets by recognizing terminal galactose or *N*-acetylgalactosamine (GalNAc) residues (Deppermann et al., 2020; Stockert, 1995) but has not been associated with the recognition of any pathogens.

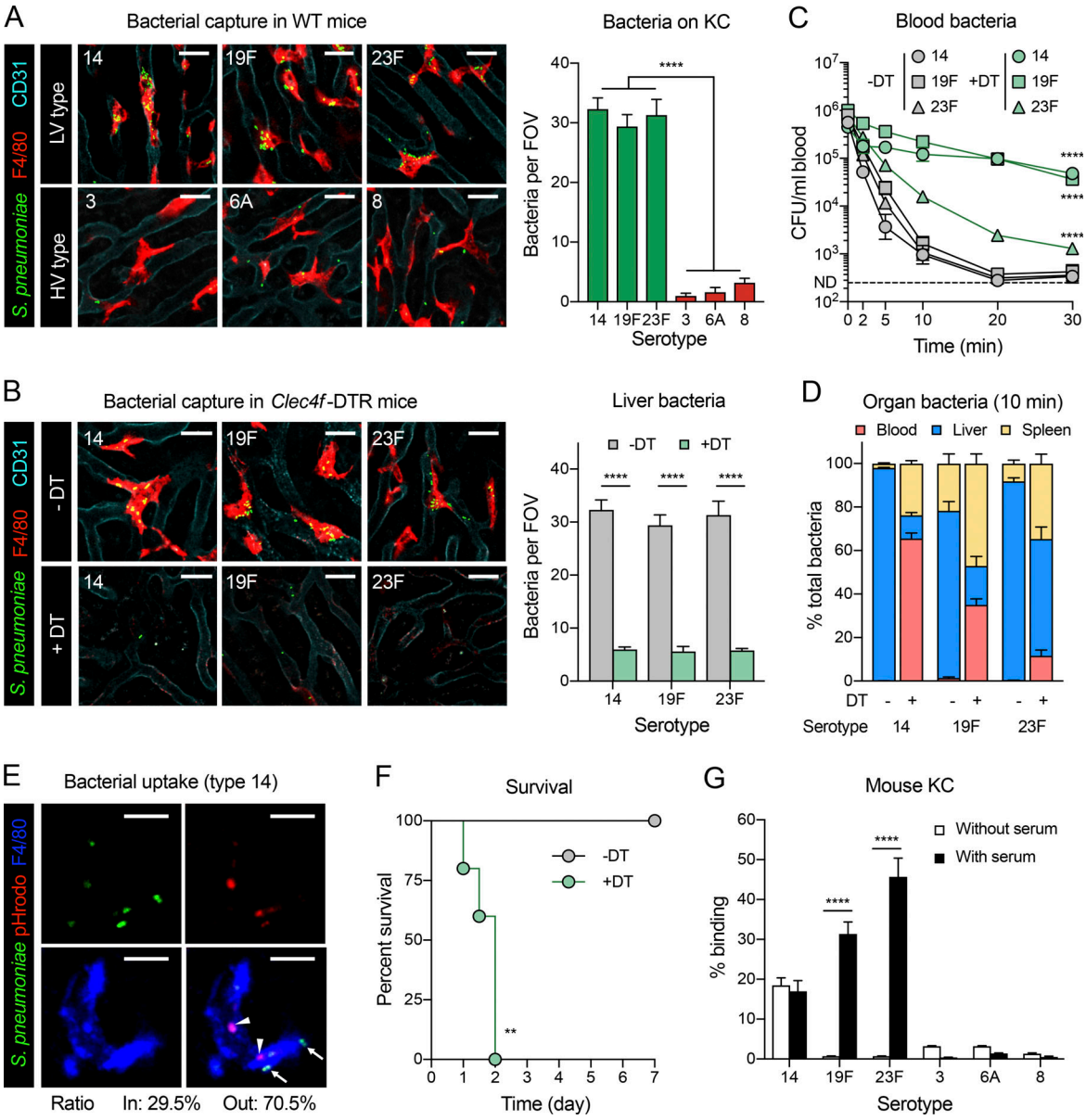

Figure 6. **Capture of LV encapsulated pneumococci by KCs. (A)** Representative IVM images of the liver sinusoids of mice (n = 3) 10 min after i.v. infection with 5 × 10^7 CFU of isogenic TH870 derivatives producing the LV (type 14, 19F, and 23F) or HV (type 3, 6A, and 8) capsule variants (left). Scale bar, 20 µm. Bacterium-capture capacity of KCs are presented as KC-associated bacteria per FOV (right, n = 5–10 random fields). **(B)** IVM visualization of liver captured LV pneumococci in the KC-deficient mice (n = 3). Scale bar, 20 µm. Hepatic captured bacteria are quantified as numbers per FOV (right, n = 5–10 random fields). **(C)** Bacteremia kinetics of LV isogenic TH870 derivatives (type 14, 19F, and 23F) during the first 30 min after infection with 10^6 CFU in *Clec4f*-DTR mice were treated with (+) or without (–) DT. n = 5–10. **(D)** Proportional distribution of viable LV isogenic TH870 derivatives (type 14, 19F, and 23F) in the blood, liver, and spleen 10 min after infection in *Clec4f*-DTR mice pretreated with (+) or without (–) DT. n = 3–6. **(E)** Representative IVM images (left) showing the LV $TH870^{14}$ outside (arrow) and inside (arrowhead) of KCs (blue) 20 min after i.v. inoculation of 10^8 CFU. Scale bar, 10 µm. Intracellular bacteria were detected by the activation of pH-sensitive dye pHrodo (red). The ratio of intra- and extracellular bacteria was quantified (right, n = 10 random fields). **(F)** Survival of KC-depleted mice after i.v. infection with 10^8 CFU of $TH870^{14}$. n = 5. **(G)** Evasion of mouse KC capture by the HV capsule types of pneumococci. Freshly isolated primary KCs were used to test bacterial adherence with TH870 derivatives of representative LV (14, 19F, and 23F) and HV (3, 6A, and 8) capsule types. Bacterium-binding levels were calculated by dividing the KC-associated bacterial numbers to the total bacterial doses. n = 3. All mice were used in C57BL/6 background. Data were representative results (A, B, E, and G) or pooled (C, D, and F) from two independent experiments. Ordinary one-way ANOVA with Tukey's multiple comparisons test (A), two-way ANOVA with Sidak's (B and G) or Tukey's (C) multiple comparisons test, log-rank test (F), **, P < 0.01, ****, P < 0.0001.

Consistent with an accessory role of the ASGR2 subunit in ASGR (Shia and Lodish, 1989), additional expression of ASGR2 in the ASGR1 transfectants further boosted adherence of $TH870^{14}$, although expression of ASGR2 alone did not result in obvious pneumococcal binding (Fig. 8 C). Further analysis revealed specific binding of murine ASGR (mASGR) to pneumococci of serotype 7F but not any of the other 13 types tested thus far (Fig. 8 D).

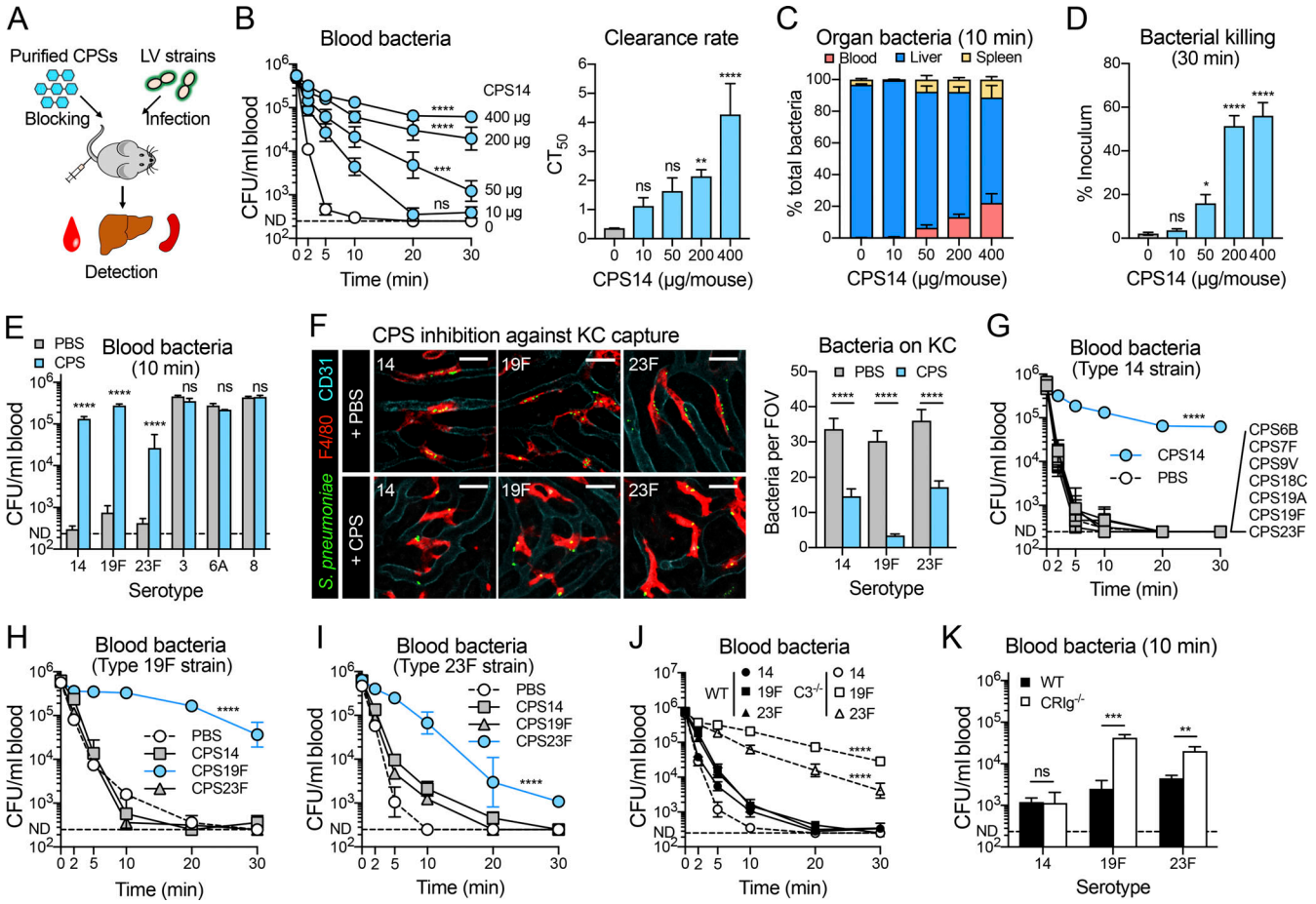

Figure 7. **Serotype-specific inhibition of bacterial clearance by free CPSs. (A)** Schematic illustration of CPS treatment. **(B–D)** Blockage of TH870[14] clearance and hepatic capture with CPS14. Mice were treated i.v. with PBS or purified type 14 CPS 2 min before infection with TH870[14] and used to assess bacterial clearance as in Fig. 3 E, hepatic capture as in Fig. 3 F, and bacterial killing as in Fig. 3 J. *n* = 3–6. **(E)** Inhibition of pneumococcal clearance by CPS of LV but not HV serotypes. Mice pretreated with 400 µg of CPSs were infected with homologous serotypes and assessed for bacterial load in the blood at 10 min as in B. *n* = 3–6. **(F)** Visualization of inhibitory effect of CPSs on KC capture of serotype-14, -19F, and -23F pneumococci in mice pretreated with 400 µg of CPSs as in Fig. 6 A. *n* = 2. **(G–I)** Serotype-specific blocking of pneumococcal clearance in mice pretreated with one of selected LV CPSs (400 µg/mouse) and infected with serotype-14 (G), -19F (H), or -23F (I) derivatives of TH870 as in B. *n* = 3–6. **(J)** Impact of C3 deficiency on the clearance of serotype-14, -19F, or -23F pneumococci. Pneumococcal clearance in WT and $C3^{-/-}$ mice were evaluated as in B. *n* = 5–6. **(K)** Impact of CRIg deficiency on the clearance of serotype-14, -19F, or -23F pneumococci in $CRIg^{-/-}$ mice. *n* = 5–6. CD1 (B–E and G–I) or C57BL/6 (F, J, and K) mice were used. The data were representative results (F) or pooled (B–E and G–K) from two independent experiments. Two-way ANOVA with Tukey's (B, left panel, and G–J) or Sidak's (E, F, and K) multiple comparisons test, Ordinary one-way ANOVA with Tukey's multiple comparisons test (B, right panel, and D), * P < 0.05, **, P < 0.01, ***, P < 0.001, ****, P < 0.0001.

The serotype specificity of mASGR action was verified by dose-dependent inhibition with CPS7F and CPS14, but not CPS19F or CPS8 (Fig. 8 E and Fig. S4 A). Similar experiments with galactose and GalNAc, the known ASGR ligands (Stockert, 1995), showed that ASGR recognizes the terminal galactose in the repeating units of CPS7F and CPS14 (Fig. 8 E and Fig. S4 A). CPS14 was also shown to block mASGR-mediated adhesion of both serotype-14 and -7F pneumococci, but CPS7F inhibited only the adhesion of homologous serotype-7F strain. This result suggests that CPS14 is superior to CPS7F as a ligand for mASGR (Fig. 8 F). Consistent with sequence conservation between mouse and human ASGR (hASGR) proteins (Fig. S4 B), coexpression of hASGR1 and hASGR2 in CHO cells also led to serotype-specific adhesion of serotype-7F and -14 pneumococci (Fig. 8 G). Likewise, the hASGR-mediated recognition of CPS7F and CPS14 was blocked by the homologous CPSs, galactose or *N*-acetylgalactosamine (Fig. S4, C and D). The serotype-specific recognition of CPS7F and CPS14 by mASGR and hASGR was also confirmed with natural pneumococcal strains (Fig. S4, E and F). It should be noted that none of the seven HV CPSs (types 1, 2, 3, 4, 5, 6A, and 8) contains the terminal galactose in its repeating units, which agrees with the poor recognition of the HV capsule variants by KCs (Fig. 6 A). Moreover, ASGR did not show significant binding to several pneumococcal serotypes with terminal galactose in the capsules, such as 10A, 12F, 15C, 17F, and 33F. Analysis of the architectures of pneumococcal CPSs revealed that only the branched chain in CPS14 is identical to the endogenous ligand core structure Galβ1,4GlcNAc (Fig. S4 G; Li et al., 2017; Sorensen et al., 2009). The contribution of ASGR-mediated capsule recognition to KC capture of pneumococci was confirmed in vitro with KCs freshly isolated from mouse and human livers. Pretreatment of murine or human KCs with an

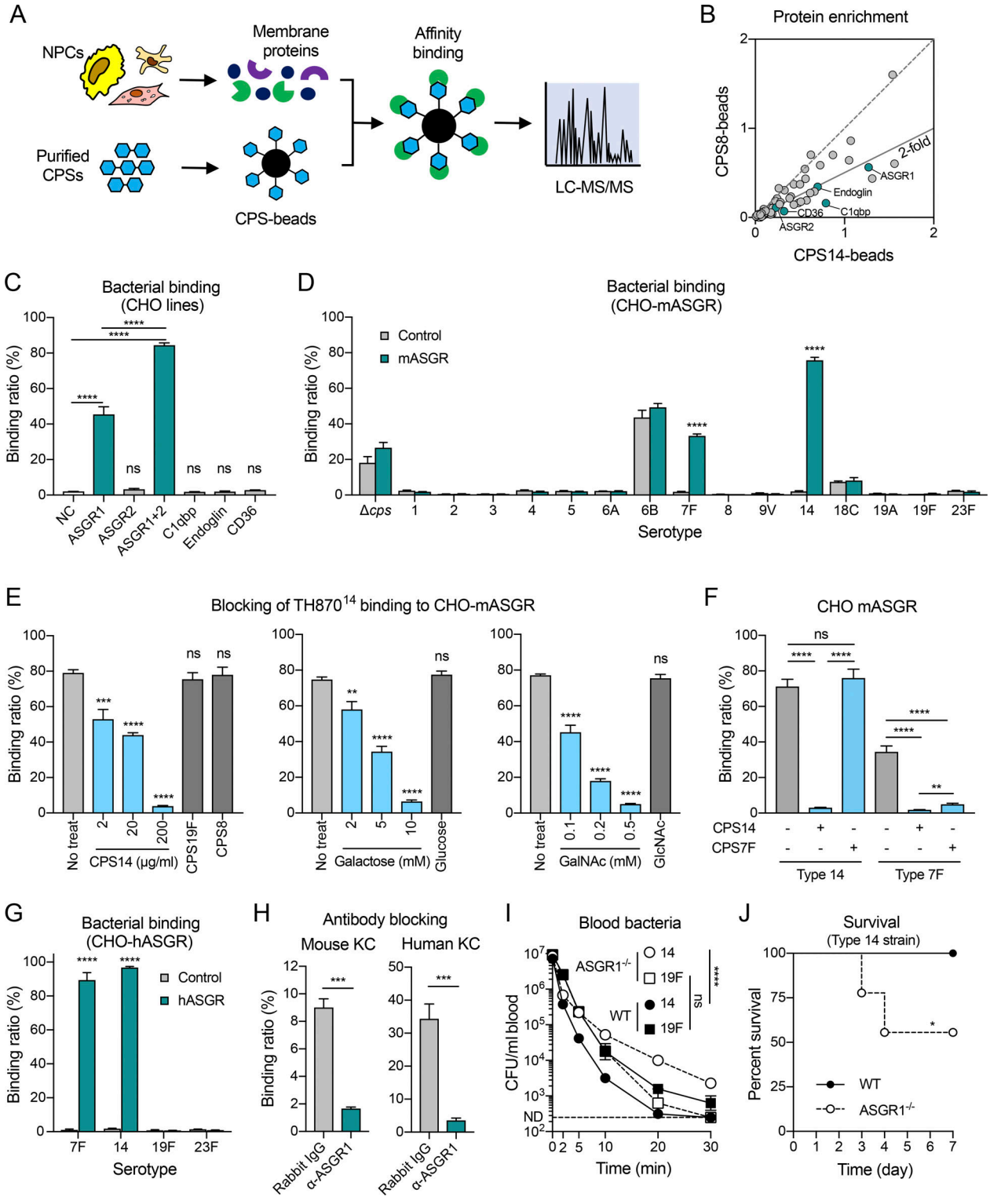

Figure 8. **ASGR-mediated KC capture of serotype-7F and -14 pneumococci. (A)** Strategy for screening CPS14-binding proteins of mouse KCs. **(B)** Plot of membrane-associated proteins significantly enriched by CPS14 beads. Solid line represents the threshold of twofold enrichment by CPS14 compared with CPS8. The top five enriched proteins with potential ligand-binding activities are labeled. **(C)** TH870^{14} adhesion to CHO cells expressing mASGR and other CPS14-binding candidates is expressed as the percentage of adherent bacteria out of the input. n = 3. **(D)** Adhesion of 15 selected serotypes to CHO-mASGR cells was measured with the TH870 derivatives as in C. n = 3. **(E)** Blocking of mASGR-mediated TH870^{14} adhesion by CPS14 and known ASGR ligands (galactose or GalNAc). n = 3. **(F)** Cross-blocking of mASGR-mediated pneumococcal adherence by CPS7F and CPS14. n = 3. **(G)** TH870^{14} adhesion to CHO cells expressing hASGR was measured as in C. n = 3. **(H)** Blocking of mouse (left) and human (right) ASGR-mediated TH870^{14} adhesion by ASGR antibodies. The antibodies and isotype IgG were added at 5 μg/ml at the same time with bacteria. n = 3. **(I)** Clearance of TH870^{14} in ASGR1$^{-/-}$ mice infected i.v. with 10^7 CFU. This dose was used because the mice showed no deficiency in TH870^{14} clearance at 10^6 CFU. n = 3–6. **(J)** Survival of ASGR1$^{-/-}$ mice after i.v. infection with 10^8 CFU of

TH870[14]. *n* = 9. All experiments were performed with C57BL/6 mice. Data were representative (C–H) or pooled (B, I, and J) results from two to three independent experiments. Ordinary one-way ANOVA with Tukey's (C, E, and F) multiple comparisons test, two-way ANOVA with Sidak's (D and G) or Tukey's (I) multiple comparisons test, unpaired *t* test (H), log-rank test (J), * P < 0.05, **, P < 0.01, ***, P < 0.001, ****, P < 0.0001.

anti-ASGR1 antibody resulted in significant reduction in cellular binding of TH870[14] (Fig. 8 H). Together, these experiments identified ASGR as a novel PRR on KCs, recognizing serotype-7F and -14 pneumococcal capsules.

Finally, we determined the contribution of ASGR to KC capture of blood-borne pneumococci in ASGR1-deficient mice. Significant impairment in the clearance of serotype-14 pneumococci was observed in ASGR1$^{-/-}$ mice (Fig. 8 I). Compared with WT mice, ASGR1$^{-/-}$ mice showed significantly higher levels of bacteremia (5.3-, 16.7-, 32.0-, and 9.2-fold) at 5, 10, 20, and 30 min, respectively. In particular, pneumococci abundantly circulated in the bloodstream of ASGR1$^{-/-}$ mice at 20 and 30 min, although WT control showed undetectable bacteremia at those time points. ASGR1$^{-/-}$ did not exhibit an obvious defect in clearing the isogenic serotype-19F bacteria (Fig. 8 I). Moreover, ASGR1$^{-/-}$ mice showed 44.4% lethality upon i.v. challenge with 10^8 CFU of TH870[14], a nonlethal dose for WT mice (Fig. 8 J). These results demonstrate that ASGR is involved in the recognition and capture of serotype-14 pneumococci by KCs in the liver of mice. It should be noted that the ASGR1$^{-/-}$ mice were relatively more capable of clearing serotype-14 pneumococci than the KC-depleted (Fig. 6 C) or CPS14-blocked (Fig. 7 B) mice. This discrepancy suggests that additional uncharacterized KC receptor(s) is also involved in the recognition of the serotype-14 capsule. Together, these data demonstrate that the C-type lectin receptor ASGR acts as a capsule recognition receptor on KCs to promote serotype-specific clearance of blood-borne pneumococci.

E. coli capsules compromise bacterial capture by KCs

Because capsule variation exists in many bacterial species, we further determined whether the capsule-mediated immune evasion against KC recognition and capture broadly operates in Gram-negative sepsis pathogens, using *E. coli* isolates from human sterile sites. Based on our pilot test of virulence phenotypes in the septic infection model (Table S1), we chose two LV (TH4509^{K2ab} and TH14508$^{KG2\text{-}1}$) and two HV (TH14515^{K1} sand TH14864^{K5}) strains for further characterization. Each of the four strains represented a unique capsule (K) type. While the LV strains were not or transiently detected in the bloodstream with virtually full survival in mice, the mice infected by HV counterparts showed rapidly rising bacteremia and 100% mortality within 24 h after i.p. inoculation (Fig. S5, A and B). To define the importance of the capsules on *E. coli* virulence in septic infection, we first tested the virulence of the acapsular mutant of the HV strain TH14515^{K1}. Intravenous inoculation of the mutant in mice did not lead to detectable bacteremia or mortality (Fig. 9 A, Δ*cps*), manifesting the importance of the K1 capsule in *E. coli* virulence.

We further assessed the relationship between capsule type and virulence phenotype by generating isogenic *E. coli* strains that differed only in the *cps* genes (Fig. S5 C). Placing the *cps* genes from the HV strain TH14515^{K1} or TH14864^{K5} converted the Δ*cps* mutant to the HV phenotype with violent bacteremia and 100% mortality (Fig. 9 A). In an opposite manner, transferring the *cps* genes from the LV strain TH4509^{K2ab} or TH14508$^{KG2\text{-}1}$ to the same recipient did not change the virulence phenotype of the mutant (Fig. 9 A). Along the same line, the isogenic K1 and K5 strains caused persistent bacteremia in the early phase of septic infection, but the K2ab and KG2-1 counterparts were rapidly cleared from the circulation (Fig. 9 B). CT_{50} values for the K1 (5.2 min) and K5 (6.3 min) strains were much longer than those for the K2ab (0.76 min) and KG2-1 (0.84 min) counterparts. These experiments demonstrate the type-specific contribution of capsules to *E. coli* virulence in septic infection.

Further investigation identified the vast majority of the "disappearing" LV strains in the liver after i.v. inoculation, but the HV strains were much less trapped in the liver (Fig. 9 C). Selective depletion of KCs but not neutrophils or inflammatory monocytes resulted in severely impaired clearance of the LV K2ab *E. coli* from the circulation (Fig. 9 D). Accordingly, the DT treatment resulted in significantly reduced LV *E. coli* cells in the liver (Fig. 9 E). Consistently, IVM revealed that the LV bacteria were much more abundantly captured by KCs than HV counterparts (Fig. 9 F and Video 6). This result shows that the virulence levels of encapsulated *E. coli* are predominantly shaped by capsule type–dependent escape of KC-mediated host defense in the liver. Although relatively small fractions of both LV and HV *E. coli* serotypes were also found in the spleen (Fig. 9 C), surgical removal of the spleen did not affect the early clearance of selected HV (type K1) or LV (type K2ab) bacteria. The overall patterns of bacterial clearance from the circulation were similar between SPX and SHM mice for K1 and K2ab bacteria in the first 30 min of septic infection (Fig. S5 D). It should be noted that asplenic mice showed modestly increased K1 bacteria in the blood (Fig. S5 E), suggesting that the spleen serves an active role in the clearance of HV *E. coli* cells that are poorly defended by the liver.

To understand the molecular mechanisms governing KC recognition of the LV *E. coli* strains, we tested the blocking effect of purified CPSs on bacterial clearance. Mice pretreated with three LV CPSs (K2ab, KG1-1, and KG2-1) significantly inhibited the clearance of the capsule type–homologous strains (Fig. 9 G and Video 7). CPS treatment extended the CT_{50} values of strains TH15511^{K2ab}, TH14978$^{KG1\text{-}1}$, and TH15991$^{KG2\text{-}1}$ from 0.7–4.3 min to 19.9–30.0 min (Fig. S5 F). The delayed clearance accompanied attenuation of bacterial capture by the liver (Fig. 9 H). Similar treatment with CPSs from the HV strains did not yield significant impact on clearance (Fig. S5 G). We further assessed cross–capsule type blocking effect on clearance of the LV strain with the heterologous CPSs. The heterologous type KG1-1 and KG2-1 CPSs showed marginal inhibition against hepatic clearance of isogenic strain TH14515^{K2ab} (Fig. 9, I and J; and Fig. S5 H). Finally, IVM imaging of the liver sinusoids revealed that

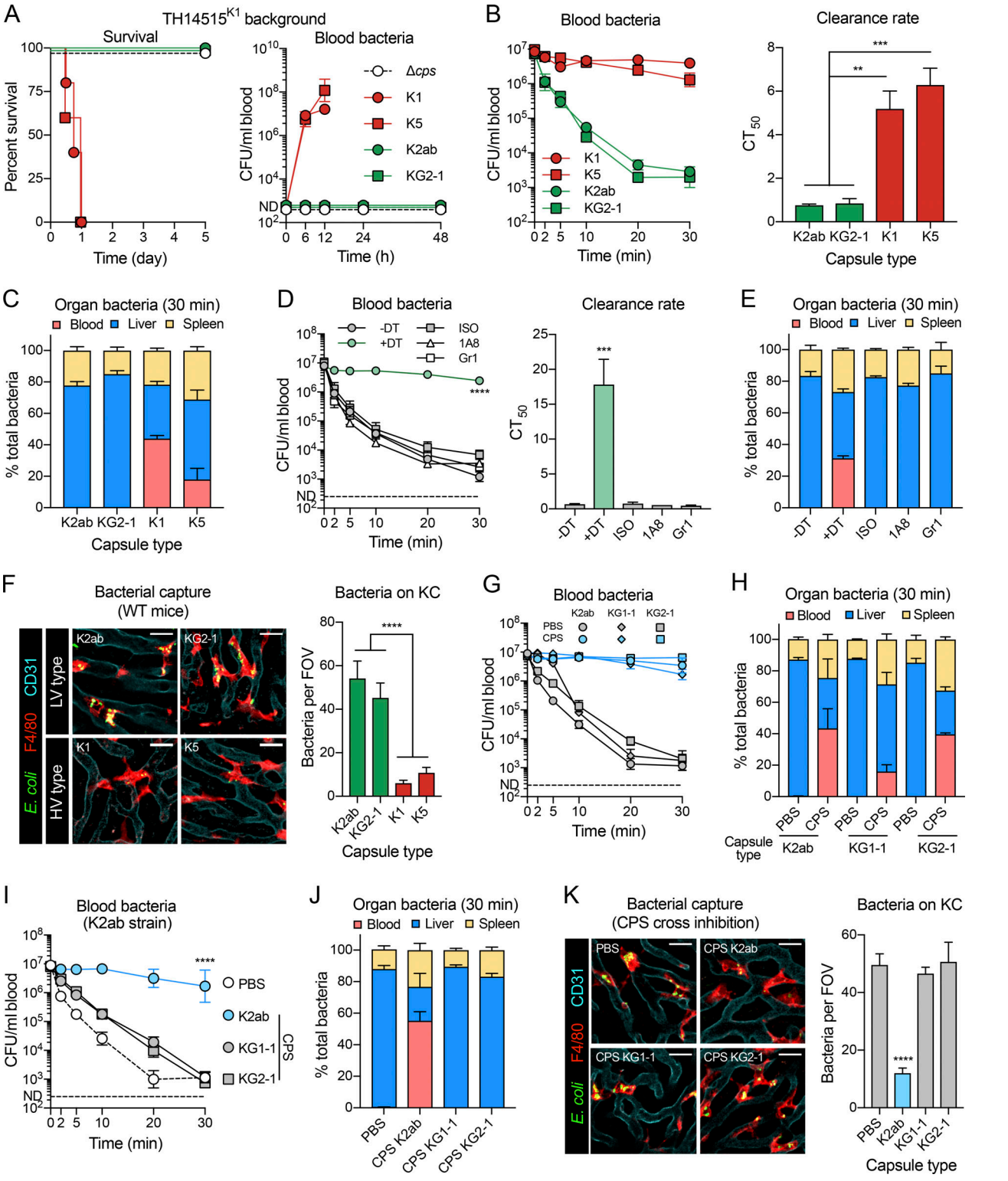

Figure 9. **Capsule type-dependent evasion of hepatic clearance of invasive *E. coli*. (A)** Capsule type-dependent virulence of invasive *E. coli* isolates. Survival (left) and bacteremia (right) levels of mice i.p. infected with 10^7 CFU of unencapsulated mutant (Δ*cps*), representative HV (K1 and K5), and LV (K2ab and KG2-1) isogenic *E. coli* in type K1 TH14515 background. $n = 5$. **(B)** Capsule type-dependent clearance of isogenic *E. coli* strains in the blood. Bacteremia kinetics (left) and calculated clearance rate (right) were measured during the first 30 min after i.v. infection with 10^7 CFU of isogenic *E. coli*. $n = 3–6$. **(C)** Proportional distribution of isogenic *E. coli* strains in the blood, liver, and spleen of mice in the first 30 min after infection as in B. $n = 3–6$. **(D)** Importance of KC, monocytes, and neutrophils in early clearance of LV type K2ab *E. coli*. Mice were treated for specific depletion as in Fig. 5 B before i.v. infection with 10^7 CFU of TH15511^{K2ab} and bled for enumeration of viable bacteria in the blood (left). The clearance rates (right) were calculated as in Fig. 4 F. $n = 3–5$. **(E)** Proportional distribution of *E. coli* TH15511^{K2ab} in the blood, liver, and spleen of mice in the first 30 min after infection. $n = 3–5$. **(F)** Capsule type-dependent evasion of KC capture by *E. coli*. Representative IVM images (left) of the liver sinusoids in the mice infected i.v. with 5×10^7 CFU of FITC-labeled isogenic *E. coli* strains ($n = 2$). The imaging data

were quantified in the right panel (n = 5–10 random fields). Scale bar, 20 µm. **(G)** Inhibition of free CPSs to the early clearance of the homologous LV *E. coli* strains. Bacterial load in the blood were measured in the mice pretreated with control PBS or 400 µg of each CPS 2 min before i.v. infection with 10^7 CFU of LV bacteria. n = 3–5. **(H)** Proportional distribution of *E. coli* in the blood, liver, and spleen of mice in the first 30 min after infection as in G. n = 3–5. **(I)** Cross-inhibition of *E. coli* capsules to the early clearance of heterologous strains. Bacterial load in the blood was measured in the mice pretreated with 400 µg of each CPS 2 min before i.v. infection with 10^7 CFU of *E. coli* TH15511^{K2ab}. n = 3. **(J)** Proportional distribution of *E. coli* in the blood, liver, and spleen of mice in the first 30 min after infection as in I. n = 3. **(K)** Visualization of inhibitory effect of LV CPSs on KC capture of *E. coli*. Representative IVM images (left) display significantly reduced LV *E. coli* captured by KCs after administration with homologous but not heterologous CPSs (n = 2). The imaging data were quantified in the right panel (n = 5–10 random fields). Scale bar, 20 µm. All mice were used in C57BL/6 background. Data were representative results (F and K) or pooled (A–E and G–J) from two independent experiments. Ordinary one-way ANOVA with Dunnett's (B and F) or Tukey's (D, right panel, and K) multiple comparisons test, two-way ANOVA with Tukey's multiple comparisons test (D, left panel, and I), **, P < 0.01, ***, P < 0.001, ****, P < 0.0001.

treatment with the homologous but not heterologous CPSs led to significant reduction in the KC-bound LV *E. coli* (Fig. 9 K). The capsule type–specific blocking indicated that the LV *E. coli* bacteria were specifically recognized by CPS receptors on KCs.

The serotype-specific recognition of LV *E. coli* capsules was further confirmed by serotype-specific role of the complement system in the early clearance of LV *E. coli*. While the removal of *E. coli* KG2-1 from the bloodstream was significantly impaired in $C3^{-/-}$ mice, the C3 deficiency accelerated the clearance of serotype K2ab (Fig. S5 I). The latter finding can be explained by the C3 retardation mechanisms of bacterial clearance from the blood circulation (Broadley et al., 2016). Consistent with the contribution of C3 in the clearance, $CRIg^{-/-}$ mice showed significant deficiency in the clearance of *E. coli* KG2-1 (Fig. S5 J). Interestingly, the early clearance of *E. coli* K2ab was also delayed in $CRIg^{-/-}$ mice (Fig. S5 J), which was in line with the requirement of CRIg in the slow-track clearance of blood bacteria as reported previously (Broadley et al., 2016). Lastly, we tested potential recognition of LV *E. coli* capsules by ASGR using hASGR1-expressing CHO cells. No significant adhesion was detected among 20 *E. coli* invasive isolates tested thus far (representing 13 capsule types; data not shown). Together, these data highlight the importance of molecular interactions between the capsules and KCs in shaping the outcomes of septic infections by Gram-negative sepsis pathogens.

Discussion

Capsules are an essential virulence factor in many encapsulated bacteria and fungi. A large body of literature has characterized capsules as antiphagocytic structures (Comstock and Kasper, 2006; Paton and Trappetti, 2019; Wen and Zhang, 2015), but it remains unknown which host tissue site is primarily targeted by capsules during systematic infection. This study uncovers the liver as the major organ where capsules maximally excise their virulence-enabling function. The liver has been shown to be a major organ to trap invading bacteria (Benacerraf et al., 1959; Brown et al., 1981a; Gregory et al., 1996; Mackaness, 1962; Martin et al., 1949; Rogers, 1956). We have verified that acapsular *S. pneumoniae* and *E. coli* are rapidly cleared from the bloodstream in the early phase of septic infections. However, encapsulated bacteria remain in the circulation in a capsule type– and infection dose–dependent manner. The capsule-mediated evasion of hepatic clearance allows encapsulated bacteria to survive and proliferate in the blood circulation and leads to uncontrolled bacteremia and septic death. These findings provide a conceptual explanation for the dominance of encapsulated bacteria in human septic infections.

KCs constitute ∼90% of total tissue macrophages in the body (Bilzer et al., 2006), with well-known function in capturing blood-borne bacteria (Broadley et al., 2016; Gola et al., 2021; Helmy et al., 2006; Kolaczkowska et al., 2015; Lee et al., 2010; Surewaard et al., 2016; Wong et al., 2013; Zeng et al., 2016) and fungi (Sun et al., 2019). This work reveals that the antibacterial function of KCs is differentially compromised by various types of capsules in *S. pneumoniae* and *E. coli*. The HV capsule types are extremely capable of circumventing KC capture, which is manifested by sustained bacteremia in mice and relatively poorer binding of primary human and mouse KCs to HV capsules. The uneven contribution of KCs to the clearance of pneumococcal serotypes also explains the previous finding that macrophage depletion with clodronate liposomes yields variable levels of impact on the clearance of different pneumococcal serotypes/strains (Gerlini et al., 2014).

This study has shown that KCs are able to recognize the LV capsules via capsule type-specific receptors. This is exemplified by our discovery of ASGR as the KC receptor for pneumococcal serotype-7F and -14 capsules. ASGR is exclusively expressed in the liver (Fagerberg et al., 2014; Monroe and Huber, 1994), particularly on hepatocytes and KCs (Azimifar et al., 2014; Consortium et al., 2018; MacParland et al., 2018). While it is known that KCs use ASGR to internalize galactosylated particles (Dong et al., 2008; Kolb-Bachofen et al., 1982) and desialylated platelets (Deppermann et al., 2020; Li et al., 2017; Sorensen et al., 2009), ASGR has not been previously associated with microbial recognition. Multiple lectin receptors have been shown to recognize capsules, such as SIGN-R1 (Kang et al., 2006; Kang et al., 2004; Koppel et al., 2005) and MRC-1 (McGreal et al., 2006; Subramanian et al., 2019; Zamze et al., 2002). However, none of these receptors have been linked to KC-specific recognition of encapsulated pathogens. To the best of our knowledge, ASGR is the first known KC-specific receptor that recognizes bacterial capsules.

Our data indicate that the major complement receptor CRIg on KCs is involved in KC recognition of LV capsules in a serotype-dependent manner. CRIg is specifically expressed by KCs (Helmy et al., 2006) and promotes KC capture of C3-opsonized bacteria (Broadley et al., 2016; Helmy et al., 2006; Zeng et al., 2016). We have revealed that CRIg-deficient mice are partially disabled in capturing isogenic pneumococci producing serotype-19F and -23F, but not -14, capsules. Accordingly, a similar serotype-dependent pattern in KC capture is manifested

in C3$^{-/-}$ mice. Given the relatively poor deposition of C3 on bacterial capsules (Fine, 1975; Hyams et al., 2010), we postulate that C3 promotes CRIg binding to C3-opsonized encapsulated bacteria once C3 is activated on the bacterial surface. Previous studies have identified numerous soluble lectins in the plasma that recognize capsules, which activate C3 via the lectin complement activation pathway. In particular, ficolins of human and mouse recognize specific motifs on certain capsules of *S. pneumoniae* (Brady et al., 2014; Geno et al., 2018; Krarup et al., 2005) and many other bacteria (Aoyagi et al., 2005; Aoyagi et al., 2008; Hummelshoj et al., 2012; Krarup et al., 2005). It is possible that capsule-binding soluble lectins promote C3 deposition and activation on the bacterial surface and thereby enhance C3-mediated opsonophagocytosis of encapsulated bacteria via CRIg.

While some studies suggest that KCs directly kill microorganisms trapped in the liver (Benacerraf et al., 1959; Klein et al., 1994), others report that KCs lack the capacity of generating reactive oxygen radicals upon infection-associated signals (Lepay et al., 1985) and are unable to kill bacterial and protozoal pathogens taken up in the liver (Gregory et al., 2002; Gregory et al., 1996; Lepay et al., 1985). In the latter cases, neutrophils are described as the major helper to kill the microbes captured by KCs (Gregory et al., 2002; Gregory et al., 1996; Kolaczkowska et al., 2015). Our data strongly suggest that KCs are able to kill the bacteria attached to their surface without help of other professional phagocytes in the early phase of septic infections. The total bacteria in the liver were dramatically diminished in the first 30 min after i.v. inoculation in the absence of neutrophils and inflammatory monocytes, a time window far before massive recruitment of neutrophils upon blood-borne bacterial infection (Gregory et al., 1996). The bactericidal activity of KCs is also indicated by our observation that KCs take up LV pneumococci in the liver sinusoids.

Capsule types have been associated with disease potential of many encapsulated pathogens (Briles et al., 1992; Hyams et al., 2013; Robbins et al., 1974; White, 1938). However, genetic heterogeneities among bacterial strains and patients, as well as host immunological conditions, have precluded the establishment of a causal relationship. By using isogenic capsule variants, we have demonstrated a decisive role of capsule types/structures in shaping the survival and virulence potential of encapsulated bacteria in mice. At a given infection dose (10^6 CFU i.v. for *S. pneumoniae*, 10^7 CFU i.v. for *E. coli*), certain capsular types always confer the HV phenotype (e.g., *S. pneumoniae* serotypes 1–5 and *E. coli* serotypes K1 and K5), whereas the bacteria with other capsules constantly display the LV phenotype (*S. pneumoniae* serotypes 14 and 19F and *E. coli* serotypes K2ab and KG2-1). It should be noted that the LV capsules can overwhelm the KC-mediated defense and confer the HV phenotype at high infection doses, which may represent the situation when large numbers of encapsulated LV bacteria in local infections (e.g., pneumonia and peritonitis) continue to seed in the bloodstream and overrun the capacity of KC-mediated defense. The immune evasion conferred by the LV capsules appears to be accomplished by capsule coverage of multiple "vulnerable" pathogen-associated molecular patterns on the cell membrane/wall from be detected by the PRRs, such as lipoproteins, lipoteichoic acids, peptidoglycan, and LPS (Medzhitov, 2007). Molecular recognition of the LV capsules by KCs seems to represent a trade-off effect.

While the spleen is important for host defense against *S. pneumoniae* and other encapsulated bacteria (Bogart et al., 1972; Brown et al., 1981b; Leung et al., 1972; Shinefield et al., 1966; Whitaker, 1968), the precise mechanisms of this splenic immunity remain to be fully defined. This work demonstrates that the spleen is important for clearance of the HV serotypes that are poorly recognized by liver macrophages, but this famous immune organ is dispensable to natural defense against LV capsules because of effective clearance of LV serotypes in the liver. Our finding is consistent with the neutrophil-driven clearance of HV pneumococci (e.g., serotype-2 D39) in the spleen (Deniset et al., 2017). The striking difference between the liver and spleen in the capacity of clearing blood-borne bacteria appears to be determined by the receptors uniquely or differentially expressed by KCs and splenic cells. This notion is supported by serotype-specific capture of LV *S. pneumoniae* and *E. coli* serotypes by KCs. Although the immune cells responsible for the clearance of encapsulated bacteria in the spleen remain to be defined, splenic macrophages are likely involved in this function. Deniset et al. (2017) have identified red pulp macrophage as the major phagocyte to capture HV pneumococci in the spleen of mice, which agrees with the observation that *Leishmania* infection–induced proliferation of red pulp macrophages in mice protects septic infection of HV pneumococci (Kirby et al., 2009). Splenic marginal zone macrophages have been shown to recognize pneumococcal capsules by the SIGN-R1 lectin receptor (Kang et al., 2006; Kang et al., 2004; Lanoue et al., 2004). Interestingly, CD169$^+$ metallophilic macrophages in the marginal zone of the spleen permit intracellular proliferation of HV pneumococci, which allows resurrection of bacteremia after the blood is sterilized (Ercoli et al., 2018). The importance of the spleen in the defense of HV serotypes warrants future investigations on the precise contributions of various splenic resident macrophages.

Although this work focuses on the early phase of blood-borne infections by encapsulated bacteria, the mechanisms governing the capsule interactions with KCs can have profound implications for the understanding of pneumococcal pneumonia and other bacterial diseases often leading to septic infections. Approximately 50% of patients with pneumococcal pneumonia develop bacteremia, and bacterial dissemination to the blood is associated with severe disease and prognosis (Musher and Thorner, 2014). Our data strongly suggest that bacterial serotype and the health conditions of the liver and spleen are among the decisive risk factors for transforming pneumococcal primary infection in the lungs into a septic infection. The abundant presence of pneumococci in the liver, but not in the blood, of mice infected i.t. with LV serotypes indicates that the LV pneumococci disseminated from the lungs are effectively cleared in the liver, which prevents bacterial proliferation in the blood and lethality. Hypersusceptibility of KC-depleted mice to a sublethal infection with LV pneumococci is consistent with the fact that the individuals with chronic liver diseases are associated with higher risk of developing sepsis with bacteremia (Ashare et al., 2009; Foreman et al., 2003). In sharp contrast,

severe bacteremia, poor bacterial deposition in the liver, and 100% mortality in mice infected i.t. with HV pneumococci corroborate our finding in the septic infection model that HV capsules prevent hepatic clearance of invading bacteria. Consistent with the importance of the spleen in the defense against HV pneumococci (Deniset et al., 2017), the spleen carries more bacteria than the liver in mice infected with the HV pneumococci.

In summary, this work reveals that the liver serves as the frontline immune organ to defend blood-borne infections of acapsular and LV encapsulated bacteria via KC-mediated pathogen recognition mechanisms, but hepatic function is severely compromised by HV capsules, leaving the spleen as the major immune organ to control relatively low levels of septic infections by HV serotypes. In the context of the success in the prevention of invasive pneumococcal disease by CPS-based vaccines (Briles et al., 2019), these findings have provided molecular and cellular insights into potential mechanisms governing the immunoprotection efficacy of the pneumococcal vaccines in controlling infections of *S. pneumoniae*. It is tempting to hypothesize that vaccine-elicited antibodies against pneumococcal capsules, particularly HV serotypes, makes HV pneumococci more approachable by KCs and/or splenic immune cells.

Materials and methods

Bacterial strains and cultivation

All of the *S. pneumoniae* and *E. coli* strains used in this study are described in Table S3. Pneumococci were cultured in Todd-Hewitt broth with 0.5% yeast extract or tryptic soy agar plates with 3% defibrinated sheep blood at 37°C with 5% CO_2 as described (Lu et al., 2006). *E. coli* strains were grown in Luria-Bertani (LB) broth or agar plates at 37°C under aerobic conditions. Antibiotics were added when necessary at the following concentrations: 400 µg/ml for kanamycin, 150 µg/ml for streptomycin, 4 µg/ml for chloramphenicol, 5 µg/ml for gentamycin, 200 µg/ml for apramycin, and 300 µg/ml for spectinomycin.

Bacterial mutagenesis

The materials and procedures used to generate *S. pneumoniae* and *E. coli* mutants are described in Table S3. Pneumococcal capsule-switch strains were constructed by natural transformation as described (Li et al., 2016). Briefly, each background strain was first converted to gain streptomycin resistance by transformation with the *rpsL1* allele (Sung et al., 2001). The capsule biosynthesis genes in the *cps* locus were then replaced by the Janus Cassette (JC) using the amplicons of the up- and downstream sequences with strain-specific primers to generate the Δ*cps*::JC background strains, which were used to generate unmarked *cps* deletion mutant with the fusion PCR segments of the up- and downstream arms by counterselection with streptomycin as described in Table S3. For capsule switching, the sequence of each target *cps* locus between the *dexB* and *aliA* genes along with the up- and downstream sequences (~3 kb each) was amplified from genomic DNA of the donor strains using PrimeSTAR GXL DNA polymerase (Takara) and primers as described in Table S3 and used to transform the Δ*cps*::JC mutants. To improve transformation efficiency, before amplification of the target *cps* loci, a chloramphenicol-resistant *cat* gene was inserted at the 3′ end of the *aliA* gene in the donor genomes by transformation with the fusion fragments as described in Table S3, except serotype 5 strain TH2940, which was constructed with kanamycin-resistant *kan* gene. The *cat* and *kan* markers were amplified from plasmid pEVP3 and the JC segment with primers Pr12140/Pr12141 and Pr12618/Pr12619, respectively, and then fused to the 5′ and 3′ flanking sequences of each target locus as described in Table S3. The capsule-switching transformants were selected on tryptic soy agar blood plates in the presence of streptomycin and chloramphenicol, except serotype 5 transformants that were selected with streptomycin and kanamycin. In some cases, capsule-switching strains were obtained by transformation with genomic DNA of the donor strains when repeated trials did not yield desirable transformants with the donor *cps* amplicons, which were backcrossed at least three times before being used for any experimentation as described previously (Trzcinski et al., 2003). The serotypes of all derivatives were genotypically confirmed by PCR and DNA sequencing with diagnostic primer sets as described previously (Pai et al., 2006).

E. coli capsule-switching strains were constructed in the TH14515 (K1) background in a manner similar to that described previously (Wang et al., 2018a) and illustrated in Fig. S5 C. In brief, the Cas9 encoding plasmid pCasKP-apr was introduced into recipient strain TH14515 by electroporation. The resulting Cas9-positive strain TH15325 was maintained at 30°C with apramycin and transformed with the spacer-containing plasmid pTH15353, which contained the up- and downstream homologous sequences of the *cps* locus of the recipient strain at 30°C in the presence of apramycin and spectinomycin, resulting in strain TH15399. TH15399 was used to generate the *cps*-null mutant TH15403 by curing both the plasmids cultivation at 37°C (pCasKP-apr) in the presence of 5% sucrose (pTH15353), or to produce the isogenic capsule type switching strain TH15401 by curing pTH15353 with sucrose. To improve transformation efficiency, a transitional strain was generated for each *cps* donor sequence by inserting the 5′ and 3′ arm sequences (1.5 kb each) of the donor and recipient *cps* loci in the *cps* locus of TH15401. Specifically, the 5′ and 3′ arm sequences of the recipient and donor *cps* loci, as well as the plasmid pTH15358, were amplified with the primers outlined in Table S3; the five amplicons linked with the NEB Assembly Mix and electroporated into TH15401. The pSGKP-spe derivatives were cured by incubating the bacteria at 30°C in the presence of apramycin and 5% sucrose. Donor *cps* sequences were amplified from the donor genomes with the primers outlined in Table S3 and the spacer-containing plasmid were outlined in Table S3. Capsule-switched recombinants were constructed by coelectroporation of corresponding donor *cps* sequences and spacer-containing plasmid into the corresponding transitional recipient strains. Capsule-switched recombinants were selected on LB plate with apramycin and spectinomycin, and these two plasmids were cured as mentioned before. The accuracy of all the genetic constructs was confirmed by PCR amplification.

E. coli genome sequencing

E. coli genomes were sequenced as described previously (Li et al., 2012). Genomic DNA was extracted using the HiPure Bacterial DNA Kit according to the manufacturer's instructions (Magen) and used to generated genomic libraries by VAHTS Universal DNA Library Prep Kit for Illumina for DNA sequencing on the Illumina NovaSeq 6000 platform with 150-bp paired-end modules. The raw reads were filtered to remove low-quality reads and assembled by SPAdes genome assembler v3.14.1. The *E. coli* K-antigen serotype was determined through web Basic Local Alignment Search Tool (BLAST). The sequences of *cps* loci were aligned to the standard database Nucleotide collection (nr/nt) using Megablast with default parameters. The K-antigen group was defined according to specific genes in group 1 (*wzi* and *wzy*), group 2 or 3 (*kpsF*, *kpsE* and *kpsM*), and group 4 (*wzy*). Individual K-type was designated based on the identity of the *cps* sequence to previously reported serotypes. In certain cases, the *cps* sequences cannot be aligned to any defined *cps* locus in *E. coli*, and these new types were designated as KG1-1 (K-antigen in group 1, number 1, GenBank accession MZ339221) and KG2-1 (MZ339219) in this study, respectively.

Mouse infection

All infection experiments were conducted in sex-matched C57BL/6 or CD1 mice (6–8 weeks old) according to the animal protocols approved by the Institutional Animal Care and Use Committee in Tsinghua University. All of the knockout/in mice were maintained on the C57BL/6 background. *Clec4F*-DTR mice were generated as described previously (Scott et al., 2016). $C3^{-/-}$ and $ASGR1^{-/-}$ mice were purchased from The Jackson Laboratory and Cyagen, respectively. $CRIg^{-/-}$ mice (Helmy et al., 2006) were acquired from Genentech.

Septic infections were carried out by i.p. or i.v. injection essentially as described previously (Wang et al., 2018b). Lung infections were performed by i.t. inhalation after anesthesia. In brief, bacterial inoculum was prepared by resuspending frozen stocks in Ringer's solution to desirable concentrations based on the predetermined CFU for each stock. Precise concentrations were determined by plating the inoculum immediately before infection. Desirable bacterial CFU were inoculated in a final volume of 200 µl for i.p., 100 µl for i.v., or 30 µl for i.t. infection. A higher infection dose of *E. coli* strains (i.p. 10^7 CFU) than *S. pneumoniae* (i.p. 10^4 CFU) was used for virulence assessment because the former were generally less virulent in the sepsis model.

Bacteria in the bloodstream were assessed by retroorbital bleeding and CFU plating. CT_{50} was calculated by nonlinear regression analysis of bacteremia kinetics for individual strains using the formula $T = \ln(1 - 50/\text{plateau})/(-K)$, in which plateau and K were generated by one-phase association of the clearance ratio using GraphPad Prism. CT_{50} was designated as 30 min if less than half of the inoculum was cleared from the blood. Total viable bacteria burden in each animal was calculated as the sum of CFU values in the blood and major organs. Bacteria in the liver, spleen, lung, kidney, and heart were measured by CFU plating of tissue homogenates and presented as CFU per organ. Animal survival was recorded in a 7-d period or at a humane endpoint (body weight loss >20%). Competitive inhibition of bacterial clearance in the circulation of mice was similarly performed by i.v. injection purified CPSs 2 min before i.v. inoculation of encapsulated bacteria.

Splenectomy

SPX mice were prepared as described (Coil et al., 1978). The mice were anesthetized with 400 mg/kg of avertin (Sigma-Aldrich) and received 8 mg/kg of meloxicam (Sigma-Aldrich) before surgery. The peritoneum was opened on the left side to suture the spleen pedicle before removing the spleen and closing the peritoneum. SHM mice were treated in the same manner without removing the spleen. All animals were allowed to recover for ≥10 days before infection.

IVM

IVM imaging of mouse liver was carried out with inverted confocal laser scanning microscopy as described (Wang and Kubes, 2016). The hepatic microvasculature and KCs were visualized by i.v. injection of 2.5 µg AF594 anti-CD31 and AF647 anti-F4/80 antibodies, respectively, 30 min before i.v. inoculation with 5×10^7 CFU of FITC-labeled *S. pneumoniae* or *E. coli*. Images were acquired with Leica TCS SP8 confocal microscope using 10×/0.45 NA and 20×/0.80 NA HC PL APO objectives. The microscope was equipped with Acousto Optics without filters. Fluorescence signals were detected by photomultiplier tubes and hybrid photo detectors (600 × 600 pixels for time-lapse series and 1,024 × 1,024 pixels for photographs). Three laser excitation wavelengths (488, 585, and 635 nm) were employed by white light laser (1.5 mw, Laser kit WLL2, 470–670 nm). Real-time imaging was monitored for 2.5–5 min after infection. Five to 10 random fields of view at 10 min were selected to calculate the bacteria number per field of view.

Fluorescence labeling

S. pneumoniae and *E. coli* strains were labeled with FITC as described (Wright and Jong, 1986) with minor modifications. Briefly, 10^8 CFU of bacteria were suspended in 1 ml PBS containing 200 µg/ml FITC (Sigma-Aldrich) and incubated for 30 min at room temperature (RT) in the dark. The FITC-labeled bacteria were washed three times with 0.5 ml PBS to remove unbound FITC. pHrodo-labeled pneumococci were prepared according to the manufacturer's instructions with the exception of using 0.001 mM pHrodo Red dye instead of 0.5–1.0 mM suggested by the manufacturer.

Immune cell depletion

Neutrophils and neutrophils/inflammatory monocytes were depleted by i.p. injection of 500 µg anti-Ly6G antibody (clone 1A8; BioXCell) and 500 µg anti-Ly6G/Ly6C antibody (Gr1; clone NIMP-R14; BioXCell), respectively, 24 h before infection as described previously (Xiong et al., 2015). The same dose of isotype-matched IgG was used as a negative control. Specific depletion of KCs was achieved by i.p. injection of 10 ng/g DT in the *Clec4F*-DTR mice 24 h before infection as described previously (Scott et al., 2016). The depletion efficiencies were verified by flow cytometry as shown in Fig. S2, E and F.

Isolation of liver NPCs

Liver NPCs were isolated by a collagenase-DNase digestion procedure as described (Li et al., 2014). In brief, mice were euthanized, and liver was perfused from the portal vein with 5 ml of digestion buffer (HBSS with 0.5 mg/ml collagenase IV, 20 µg/ml DNase I, and 0.5 mM $CaCl_2$). The liver was excised, minced into small pieces (<2 mm), suspended in 10 ml digestion buffer, and incubated at 37°C for 30 min with constant rotation at 300 rpm. The homogenate was filtered through a 70-µm strainer and chilled on ice for 5 min, then washed by centrifugation and resuspension in ice-cold HBSS. Residual red blood cells were lysed by resuspending the pellet in 1 ml RBC lysis solution (BioLegend) and incubated on ice for 1 min before the reaction was terminated with HBSS. The cell suspension was then centrifuged at 50 *g* for 2 min at 4°C to collect the top aqueous phase containing NPCs. Human liver sections were similarly processed without perfusion. For in vitro bacteria-binding assay, the NPCs were resuspended in RPMI 1640 without FBS and seeded into 96-well cell culture plate at 5×10^4 cells/well. KCs were enriched by cellular adherence to the plastic surface after incubation at 37°C, 5% CO_2 for 15 min. Nonadhering cells were removed by gently washing with RPMI 1640. This procedure typically yielded 1×10^4 cells/well for KCs that were used immediately for bacterial binding experiments. Otherwise, the NPCs were used for flow cytometry analysis without adherence. Human liver sections were obtained from freshly disposed tissues of liver surgery or transplantation patients with approval by the Human Subject Study Committee of the Strategic Support Force Medical Center (K2021-012-01).

Flow cytometry

Flow cytometry was carried out essentially as described (Scott et al., 2016). Mouse liver NPCs (1×10^6) or blood immune cells from 200 µl whole blood were blocked for 10 min in 50 µl FACS buffer (PBS with 3% FBS) with 1% anti-CD16/32 antibody, followed by staining for 20 min with APC-Cy7 anti-CD45 (1/200), APC anti-CD31 (1/200), BV605 anti-CD11b (1/500), FITC anti-F4/80 (1/200), PB anti-Ly6C (1/500), and PE anti-Ly6G (1/500). Before analysis, cells were stained with 5 µl 7-AAD for viability test. Viable cell populations were gated as KCs ($CD45^+CD31^-CD11b^{low}F4/80^{high}$), splenic red pulp macrophages ($CD45^+CD11b^{low}F4/80^{high}$), inflammatory monocytes ($CD45^+CD31^-CD11b^+Ly6C^{high}Ly6G^-$), and neutrophils ($CD45^+CD31^-CD11b^+Ly6C^+Ly6G^{high}$).

Purification of CPSs

Pneumococcal and *E. coli* CPSs were purified as described with minor modifications (Kobayashi et al., 2018; Lee et al., 2020). Pneumococci were cultured to OD_{620} 0.5 in Todd-Hewitt broth with 0.5% yeast extract, and *E. coli* strains were grown overnight in nutrient-rich medium (2 g/liter KH_2PO_4, 9.7 g/liter K_2HPO_4, 1 g/liter $(NH_4)_2SO_4$, 0.1 g/liter $MgCl_2$, 0.5 g/liter sodium citrate, 10 g/liter glucose, and 2 g/liter yeast extract, pH 7.0–7.5). Bacterial cultures were chilled on ice and centrifuged at 10,000 *g* for 20 min at 4°C. The pellets were resuspended in 1/10 original culture volume in 50 mM citrate buffer (pH 4.5) with 0.1% Zwittergent 3-14 detergent (Millipore) and incubated at 42°C for 30 min. Cell debris was removed by centrifugation at 10,000 *g* for 5 min at 4°C. CPS-containing supernatants were filtered through a 0.2-µm Nalgene Rapid-Flow filter (Thermo Fisher Scientific). The solution was mixed with one-fourth volume of ethanol and stirred at 4°C for 2 h. Precipitated nucleic acids were removed by centrifugation at 10,000 *g* for 15 min at 4°C. CPSs in the supernatants were further precipitated by increasing the concentration of ethanol to 80% and incubation at 4°C for 2 h. The precipitants were collected by centrifugation at 10,000 *g* for 20 min at 4°C. The CPS pellets were air dried and resuspended in sterile H_2O. For *E. coli* CPSs, the LPSs were detoxified by incubation in 85% ethanol with 0.1 M NaOH at 37°C and subsequent neutralization with 0.1 M acetic acid. The CPSs were pelleted by centrifugation at 10,000 *g* for 20 min at 4°C, air dried, and dissolved in sterile PBS. CPSs were concentrated by ultracentrifugation with 100-kD cutoff Ultra-centrifugal Filter Unit (Merck Millipore), and concentration was measured by the phenol-sulfuric acid method (Kobayashi et al., 2018). In brief, to the standard D-glucose (concentration from 0 to 0.1 mg/ml) or CPS sample, 6% phenol and sulfuric acid were added to the tubes sequentially; absorbance at 490 nm was measured after incubating at RT for 30 min. CPS concentration was calculated according to the standard curve.

Screening of CPS14-binding proteins

Pneumococcal CPS-binding proteins were isolated from membrane proteins of the liver NPCs by an affinity screening using CPS-coated latex beads as illustrated in Fig. 8 A. The membrane proteins were prepared from murine NPCs using the Mem-PER Plus Membrane Protein Extraction Kit (Thermo Fisher Scientific) with Halt Protease and Phosphatase Inhibitor Cocktail (Thermo Fisher Scientific) according to the manufacturer's instructions. The resulting proteins were concentrated through a 3-kD cutoff Ultra-centrifugal Filter Unit (Merck Millipore), exchanged into PBS with 0.05% Tween 20 (PBST), and quantified with the BCA Assay Kit (Beyotime).

Serotype-8 and -14 CPSs of *S. pneumoniae* were separately coated onto carboxyl latex beads as described (Schlottmann et al., 2006). Briefly, 2.5 mg of the CPSs were dissolved in 2.5 ml H_2O and mixed with 200 µl of 200 mg/ml 4-(4,6-dimethoxy-1,3,5-triazin-2-yl)-4-methylmorpholinium chloride (DMTMM; Sigma-Aldrich). The mixture was incubated for 1 h on a rotator at RT. The DMTMM-modified CPSs were buffer-exchanged by ultracentrifugation through a 10-kD cutoff Ultra-centrifugal Filter Unit (Merck Millipore) into 2.5 ml PBS. The resulting DMTMM-CPSs were mixed with 1×10^9 carboxyl latex beads (2 µm; Invitrogen) and incubated on a rotator overnight at RT. The beads were washed twice with 2.5 ml PBST and stored in 2.5 ml blocking buffer (PBS with 1% BSA and 0.05% NaN_3) at 4°C in the dark.

To isolate CPS-binding proteins, 1×10^8 CPS-coated beads were mixed with 100 µg of the membrane protein preparation from the murine NPCs in 500 µl PBST containing 2 mM $CaCl_2$ and $MgCl_2$. The mixtures were rotated at RT for 1 h and washed three times with PBST by centrifugation and resuspension. The beads were resuspended in 50 µl PBST with 1 × SDS-PAGE loading buffer and heated at 100°C for 5 min to dissociate CPS-

binding proteins from the beads. Samples were spun at 12,000 *g* for 5 min at 4°C, and the supernatants were used for quantitative protein identification by mass spectrometry.

Protein mass spectrometry

Murine proteins were quantitatively identified by mass spectrometry as described (Liu et al., 2019). Samples with 40 µg total proteins were separated on SDS-PAGE gels to excise protein bands for in-gel digestion and subsequent procedures for liquid chromatography–tandem mass spectrometry analysis using a Thermo-Dionex Ultimate 3000 HPLC system combined with the Thermo Orbitrap Fusion mass spectrometer. The spectra from each liquid chromatography–tandem mass spectrometry run were searched against the mouse Unreviewed TrEMBL FASTA database (release 2020_05) using Proteome Discovery searching algorithm (v1.4). Proteins with two or more unique peptide matches were selected to calculate protein abundance, which was calculated as the median of all peptide hits belonging to the same proteins. Protein abundance was compared between the CPS14- and CPS8-coated beads, and proteins with more than twofold preference to CPS14 beads were regarded as CPS14-binding candidates.

Expression of mouse and human proteins

Expression of murine and human proteins in CHO cells was carried into pCDH or pFUGW vectors as described (Zhang et al., 2020). The full-length cDNAs of the target mouse genes were amplified from the total RNA isolated from sorted KCs using TRIzol Reagent (Invitrogen) using a Maxima H Minus First Strand cDNA Synthesis Kit (Thermo Fisher Scientific) and cloned with a His_6 tag at the C terminus. The human *ASGR1* and *ASGR2* were synthesized according to references NM_001671 and NM_001181, digested with XbaI/EcoRI, and ligated to pCDH and pFUGW, respectively. The ligation mixtures were transformed into *E. coli* DH5α and selected on LB plates with 100 µg/ml ampicillin. The recombinant plasmids were confirmed by DNA sequencing and extracted using HiPure Plasmid EF Micro Kit (Magen) for subsequent transfection. The relevant primers and resulting plasmids are listed in Table S3.

Stably expressing cell lines were constructed by lentiviral transduction. First, recombinant plasmids (either pCDH or pFUGW backbone) were transfected into HEK293T cells using Lipofectamine 2000 (Invitrogen) together with lentiviral packaging vectors pMD2.G and psPAX2 (gifts from Didier Trono at École Polytechnique Fédérale de Lausanne, Lausanne, Switzerland; Addgene). HEK293T cells were grown in DMEM with 10% FBS and 1× penicillin/streptomycin. The lentiviral particles were harvested at 48 h and filtered through a 0.45-µm syringe filter unit (Millipore) to remove cell debris. The pCDH-lentivirus was used to infect CHO cells with 8 µg/ml Polybrene (Sigma-Aldrich). The transfectants were selected with 5 µg/ml puromycin for 7 d. For coexpression, the secondary pFUGW-lentivirus was further transduced into CHO cell lines containing pCDH-lentivirus and selected under 300 µg/ml zeocin for 10 d. DNA and protein sequence analyses were carried out with the Lasergene 15.0.0 for Macintosh.

In vitro bacterial binding assay

Bacterial binding to host cells was assessed essentially as described (Zhang et al., 2000). Primary murine and human KCs were prepared in 96-well cell culture plates as described above. CHO transfectants were seeded in 48-well plates and grown to 90–100% confluence (~1.5 × 10^5 cells/well). At the time of binding experiments, growth media were replaced with basic RPMI 1640 (KCs) or F-12K (CHO cells) without serum and antibiotics. Bacteria were added at a multiplicity of infection of 1:1 in a total volume of 50 or 200 µl per well for 96- or 48-well plates, respectively, followed by centrifugation at 500 *g* for 5 min to mimic the sheer force that bacteria typically experience in the blood circulation and to maximize the contact between bacteria and host cells. As exemplified in Fig. S4 H, the mild centrifugation facilitated receptor-specific bacterial adhesion to host cells but did not affect nonspecific bacteria adhesion. For primary KCs, 10% normal mouse or human serum was added at the same time with bacteria. The mixtures were incubated for 30 min at 37°C with 5% CO_2. The unbound bacteria were enumerated by CFU plating of the supernatants after vigorous shaking 5–10 times to reduce nonspecific binding. The host cells were thoroughly washed to remove free bacteria and lysed with 50–200 µl ice-cold sterile H_2O to enumerate cell-associated bacteria by CFU plating of the lysates. Bacterial binding was calculated by dividing the cell-associated CFU by the CFU of total bacteria in the assay system. Competitive blockage of bacterial binding was accomplished by adding 20–500 µg/ml of purified CPS, 0.1–100 mM of galactose, glucose, *N*-acetyl-D-glucosamine (GlcNAc) or GalNAc, and 5 µg/ml rabbit polyclonal anti-mouse or anti-human ASGR1 antibodies and the isotype control to the medium at the same time with bacteria.

Quantification and statistical analysis

Statistical analysis was performed using GraphPad Prism software v8.0.0. All data are presented as mean ± SEM unless otherwise indicated. Unpaired *t* test was used to determine the statistical significance between two groups. One- and two-way ANOVA multiple comparisons test was used to analyze data between multiple groups. Survival curves were analyzed by log-rank test. The numbers of samples and biological replicates and P values are indicated in figure legends.

Online supplemental material

Fig. S1 shows the capsular serotype-dependent variation in the pneumococcal virulence, relating to Figs. 1 and 2. Fig. S2 illustrates the capsule-related capture of pneumococci by liver KCs, flow cytometry analysis of selective depletion efficiency, and the essential role of KCs for long-term protection against LV pneumococci, relating to Figs. 3, 5, and 6. Fig. S3 shows the serotype-specific inhibition of pneumococcal clearance by purified CPSs, relating to Fig. 7. Fig. S4 shows the specific binding of serotype-7F and -14 pneumococci to both mouse and human ASGR, relating to Fig. 8. Fig. S5 demonstrates the capsular type–dependent evasion of hepatic clearance by invasive *E. coli*, relating to Fig. 9. Table S1 summarizes the virulence phenotypes of *S. pneumoniae* and *E. coli* clinical isolates. Table S2 shows the screening result of CPS14-binding proteins by mass

spectrometry. Table S3 summarizes bacterial strains, plasmids, primers, and mutagenesis procedures in this study. Videos 1 and 2 reveal the potent KC capture of unencapsulated pneumococci, relating to Fig. 5. Videos 3 and 4 show the capsular type–dependent KC capture of LV but not HV pneumococci, relating to Fig. 6. Video 5 illustrates the inhibition of free type 14 CPSs to KC capture of serotype 14 pneumococci, relating to Fig. 7. Videos 6 and 7 show the capsular type–dependent KC capture of *E. coli* and the inhibition effect of LV type K2ab CPSs, relating to Fig. 9.

Acknowledgments

We thank Quanjiang Ji (ShanghaiTech University, Shanghai, China) for pCasKP-apr and pSGKP-spe plasmids; Wanli Liu (Tsinghua University, Beijing, China) for the CHO cells; Fen Qu (302 Hospital of PLA, Beijing, China), Yingchun Xu (Peking Union Medical College Hospital, Beijing, China), and So Hyun Kim (The Catholic University of Korea, Seoul, South Korea) for the bacterial isolates; and the Tsinghua research platforms for assistance in animal experimentation (Laboratory Animal Research Center), flow cytometry, IVM imaging (Center for Cell Biology), and protein mass spectrometry (Center for Proteomics).

This work was supported by grants from National Natural Science Foundation of China to J.-R. Zhang (31820103001 and 31530082), Tsinghua University Spring Breeze Fund to J.-R. Zhang (20201080767), and the Tsinghua-Peking Joint Center for Life Sciences Postdoctoral Foundation and the China Postdoctoral Science Foundation to H. An (2016M590085).

Author contributions: Conceptualization, H. An, J. Li, J.M. Leong, and J.-R. Zhang; experimentation, H. An, C. Qian, Y. Huang, J. Li, X. Tian, J. Feng, J. Hu, Y. Fang, F. Jiao, Y. Zeng, and X. Huang; methodology, X. Meng, Z. Zeng, Y. Chen, Y. Wu, J. Wang, X. Lin, X. Liu, Y. Chen, M. Guilliams, M.R. Oggioni, H. Deng, R. Zhang, H. Wang, and J. Wu; data analysis, H. An, C. Qian, Y. Huang, X. Tian, J. Li, H. Deng, J.M. Leong and J.-R. Zhang; composition, H. An, C. Qian, Y. Huang, J. Li, and J.-R. Zhang; funding, H. An, X. Liu, J.-W. Veening, and J.-R. Zhang.

Disclosures: M.R. Oggioni has a PhD student jointly with GSK Vaccines working on the pathogenesis of pneumonia (BBSRC grant BB/S507052/1). No other disclosures were reported.

Submitted: 29 September 2021
Revised: 22 December 2021
Accepted: 24 January 2022

References

Aoyagi, Y., E.E. Adderson, J.G. Min, M. Matsushita, T. Fujita, S. Takahashi, Y. Okuwaki, and J.F. Bohnsack. 2005. Role of L-ficolin/mannose-binding lectin-associated serine protease complexes in the opsonophagocytosis of type III group B streptococci. *J. Immunol.* 174:418–425. https://doi.org/10.4049/jimmunol.174.1.418

Aoyagi, Y., E.E. Adderson, C.E. Rubens, J.F. Bohnsack, J.G. Min, M. Matsushita, T. Fujita, Y. Okuwaki, and S. Takahashi. 2008. L-Ficolin/Mannose-binding lectin-associated serine protease complexes bind to group B streptococci primarily through N-acetylneuraminic acid of capsular polysaccharide and activate the complement pathway. *Infect. Immun.* 76:179–188. https://doi.org/10.1128/IAI.00837-07

Arshad, M., C.C. Goller, D. Pilla, F.J. Schoenen, and P.C. Seed. 2016. Threading the needle: Small-molecule targeting of a xenobiotic receptor to ablate *Escherichia coli* polysaccharide capsule expression without altering antibiotic resistance. *J. Infect. Dis.* 213:1330–1339. https://doi.org/10.1093/infdis/jiv584

Ashare, A., C. Stanford, P. Hancock, D. Stark, K. Lilli, E. Birrer, A. Nymon, K.C. Doerschug, and G.W. Hunninghake. 2009. Chronic liver disease impairs bacterial clearance in a human model of induced bacteremia. *Clin. Transl. Sci.* 2:199–205. https://doi.org/10.1111/j.1752-8062.2009.00122.x

Avery, O.T., C.M. Macleod, M. McCarty, and L Peltier. 2000. Studies on the chemical nature of the substance inducing transformation of pneumococcal types: Induction of transformation by a desoxyribonucleic acid fraction isolated from pneumococcus type III. *J. Exp. Med.* 79:137–158. https://doi.org/10.1097/00003086-200010001-00002

Azimifar, S.B., N. Nagaraj, J. Cox, and M. Mann. 2014. Cell-type-resolved quantitative proteomics of murine liver. *Cell Metabol.* 20:1076–1087. https://doi.org/10.1016/j.cmet.2014.11.002

Benacerraf, B., M.M. Sebestyen, and S. Schlossman. 1959. A quantitative study of the kinetics of blood clearance of P32-labelled *Escherichia coli* and *Staphylococci* by the reticuloendothelial system. *J. Exp. Med.* 110:27–48. https://doi.org/10.1084/jem.110.1.27

Bilzer, M., F. Roggel, and A.L. Gerbes. 2006. Role of Kupffer cells in host defense and liver disease. *Liver Int.* 26:1175–1186. https://doi.org/10.1111/j.1478-3231.2006.01342.x

Bogart, D., W.D. Biggar, and R.A. Good. 1972. Impaired intravascular clearance of pneumococcus type-3 following splenectomy. *J. Reticuloendothel. Soc.* 11:77–87

Brady, A.M., J.J. Calix, J. Yu, K.A. Geno, G.R. Cutter, and M.H. Nahm. 2014. Low invasiveness of pneumococcal serotype 11A is linked to ficolin-2 recognition of O-acetylated capsule epitopes and lectin complement pathway activation. *J. Infect. Dis.* 210:1155–1165. https://doi.org/10.1093/infdis/jiu195

Briles, D.E., M.J. Crain, B.M. Gray, C. Forman, and J. Yother. 1992. Strong association between capsular type and virulence for mice among human isolates of *Streptococcus pneumoniae*. *Infect. Immun.* 60:111–116. https://doi.org/10.1128/iai.60.1.111-116.1992

Briles, D.E., J.C. Paton, R. Mukerji, E. Swiatlo, and M.J. Crain. 2019. Pneumococcal vaccines. *Microbiol. Spectr.* 7. https://doi.org/10.1128/microbiolspec.GPP3-0028-2018

Brissac, T., E. Martinez, K.L. Kruckow, A.N. Riegler, F. Ganaie, H. Im, S. Bakshi, N.M. Arroyo-Diaz, B.L. Spencer, J.S. Saad, et al. 2021. Capsule promotes intracellular survival and vascular endothelial cell translocation during invasive pneumococcal disease. *mBio*. 12:e0251621. https://doi.org/10.1128/mBio.02516-21

Broadley, S.P., A. Plaumann, R. Coletti, C. Lehmann, A. Wanisch, A. Seidlmeier, K. Esser, S. Luo, P.C. Ramer, S. Massberg, et al. 2016. Dual-track clearance of circulating bacteria balances rapid restoration of blood sterility with induction of adaptive immunity. *Cell Host Microbe*. 20:36–48. https://doi.org/10.1016/j.chom.2016.05.023

Brown, E.J., and H.D. Gresham. 2012. Phagocytosis. *In* Fundamental Immunology. W.E. Paul, editor. Lippincott-Raven Publishers, Philadephia. 1105–1127

Brown, E.J., S.W. Hosea, and M.M. Frank. 1981a. The role of complement in the localization of pneumococci in the splanchnic reticuloendothelial system during experimental bacteremia. *J. Immunol.* 126:2230–2235

Brown, E.J., S.W. Hosea, and M.M. Frank. 1981b. The role of the spleen in experimental pneumococcal bacteremia. *J. Clin. Invest.* 67:975–982. https://doi.org/10.1172/jci110148

Brueggemann, A.B., T.E. Peto, D.W. Crook, J.C. Butler, K.G. Kristinsson, and B.G. Spratt. 2004. Temporal and geographic stability of the serogroup-specific invasive disease potential of *Streptococcus pneumoniae* in children. *J. Infect. Dis.* 190:1203–1211. https://doi.org/10.1086/423820

Chang, Q., Z. Zhong, A. Lees, M. Pekna, and L. Pirofski. 2002. Structure-function relationships for human antibodies to pneumococcal capsular polysaccharide from transgenic mice with human immunoglobulin Loci. *Infect. Immun.* 70:4977–4986. https://doi.org/10.1128/IAI.70.9.4977-4986.2002

Coil, J.A., J.D. Dickerman, and E. Boulton. 1978. Increased susceptibility of splenectomized mice to infection after exposure to an aerosolized suspension of type III *Streptococcus pneumoniae*. *Infect. Immun.* 21:412–416. https://doi.org/10.1128/iai.21.2.412-416.1978

Comstock, L.E., and D.L. Kasper. 2006. Bacterial glycans: Key mediators of diverse host immune responses. *Cell*. 126:847–850. https://doi.org/10.1016/j.cell.2006.08.021

de Cordoba, S.R., A. Ferreira, V. Nussenzweig, and P. Rubinstein. 1983. Genetic polymorphism of human C4-binding protein. *J. Immunol.* 131: 1565–1569

Deniset, J.F., B.G. Surewaard, W.Y. Lee, and P. Kubes. 2017. Splenic Ly6G^{high} mature and Ly6G^{int} immature neutrophils contribute to eradication of *S. pneumoniae*. *J. Exp. Med.* 214:1333–1350. https://doi.org/10.1084/jem.20161621

Deppermann, C., R.M. Kratofil, M. Peiseler, B.A. David, J. Zindel, F. Castanheira, F. van der Wal, A. Carestia, C.N. Jenne, J.D. Marth, and P. Kubes. 2020. Macrophage galactose lectin is critical for Kupffer cells to clear aged platelets. *J. Exp. Med.* 217:e20190723. https://doi.org/10.1084/jem.20190723

Derby, B.M., and D.E. Rogers. 1961. Studies on bacteriemia. V. The effect of simultaneous leukopenia and reticuloendothelial blockade on the early blood stream clearance of *Staphylococci* and *Escherichia coli*. *J. Exp. Med.* 113:1053–1066. https://doi.org/10.1084/jem.113.6.1053

Dong, L., S. Gao, H. Diao, J. Chen, and J. Zhang. 2008. Galactosylated low molecular weight chitosan as a carrier delivering oligonucleotides to Kupffer cells instead of hepatocytes in vivo. *J. Biomed. Mater. Res. A.* 84: 777–784. https://doi.org/10.1002/jbm.a.31328

Ercoli, G., V.E. Fernandes, W.Y. Chung, J.J. Wanford, S. Thomson, C.D. Bayliss, K. Straatman, P.R. Crocker, A. Dennison, L. Martinez-Pomares, et al. 2018. Intracellular replication of *Streptococcus pneumoniae* inside splenic macrophages serves as a reservoir for septicaemia. *Nat. Microbiol.* 3:600–610. https://doi.org/10.1038/s41564-018-0147-1

Fagerberg, L., B.M. Hallstrom, P. Oksvold, C. Kampf, D. Djureinovic, J. Odeberg, M. Habuka, S. Tahmasebpoor, A. Danielsson, K. Edlund, et al. 2014. Analysis of the human tissue-specific expression by genome-wide integration of transcriptomics and antibody-based proteomics. *Mol. Cell Proteomics*. 13:397–406. https://doi.org/10.1074/mcp.M113.035600

Feldman, C., and R. Anderson. 2020. Recent advances in the epidemiology and prevention of *Streptococcus pneumoniae* infections. *F1000Res.* 9: F1000 Faculty Rev-338. eCollection 2020. https://doi.org/10.12688/f1000research.22341.1

Fine, D.P. 1975. Pneumococcal type-associated variability in alternate complement pathway activation. *Infect. Immun.* 12:772–778. https://doi.org/10.1128/iai.12.4.772-778.1975

Finne, J. 1982. Occurrence of unique polysialosyl carbohydrate units in glycoproteins of developing brain. *J. Biol. Chem.* 257:11966–11970

Foreman, M.G., D.M. Mannino, and M. Moss. 2003. Cirrhosis as a risk factor for sepsis and death: Analysis of the National Hospital Discharge Survey. *Chest*. 124:1016–1020. https://doi.org/10.1378/chest.124.3.1016

Ganaie, F., J.S. Saad, L. McGee, A.J. van Tonder, S.D. Bentley, S.W. Lo, R.A. Gladstone, P. Turner, J.D. Keenan, R.F. Breiman, and M.H. Nahm. 2020. A new pneumococcal capsule type, 10D, is the 100th serotype and has a large cps fragment from an oral *Streptococcus*. *mBio*. 11:e00937-20. https://doi.org/10.1128/mBio.00937-20

Geno, K.A., B.L. Spencer, S. Bae, and M.H. Nahm. 2018. Ficolin-2 binds to serotype 35B pneumococcus as it does to serotypes 11A and 31, and these serotypes cause more infections in older adults than in children. *PLoS One*. 13:e0209657. https://doi.org/10.1371/journal.pone.0209657

Gerlini, A., L. Colomba, L. Furi, T. Braccini, A.S. Manso, A. Pammolli, B. Wang, A. Vivi, M. Tassini, N. van Rooijen, et al. 2014. The role of host and microbial factors in the pathogenesis of pneumococcal bacteraemia arising from a single bacterial cell bottleneck. *PLoS Pathog.* 10: e1004026. https://doi.org/10.1371/journal.ppat.1004026

Gola, A., M.G. Dorrington, E. Speranza, C. Sala, R.M. Shih, A.J. Radtke, H.S. Wong, A.P. Baptista, J.M. Hernandez, G. Castellani, et al. 2021. Author correction: Commensal-driven immune zonation of the liver promotes host defence. *Nature*. 597:131–136. https://doi.org/10.1038/s41586-021-03346-0

Gregory, S.H., A.J. Sagnimeni, and E.J. Wing. 1996. Bacteria in the bloodstream are trapped in the liver and killed by immigrating neutrophils. *J. Immunol.* 157:2514–2520

Gregory, S.H., L.P. Cousens, N. van Rooijen, E.A. Dopp, T.M. Carlos, and E.J. Wing. 2002. Complementary adhesion molecules promote neutrophil-Kupffer cell interaction and the elimination of bacteria taken up by the liver. *J. Immunol.* 168:308–315. https://doi.org/10.4049/jimmunol.168.1.308

Han, W., L. Cai, B. Wu, L. Li, Z. Xiao, J. Cheng, and P.G. Wang. 2012. The wciN gene encodes an α-1,3-galactosyltransferase involved in the biosynthesis of the capsule repeating unit of *Streptococcus pneumoniae* serotype 6B. *Biochemistry*. 51:5804–5810. https://doi.org/10.1021/bi300640b

Helmy, K.Y., K.J. Katschke Jr., N.N. Gorgani, N.M. Kljavin, J.M. Elliott, L. Diehl, S.J. Scales, N. Ghilardi, and M. van Lookeren Campagne. 2006. CRIg: A macrophage complement receptor required for phagocytosis of circulating pathogens. *Cell*. 124:915–927. https://doi.org/10.1016/j.cell.2005.12.039

Hoober, J.K. 2020. ASGR1 and its enigmatic relative, CLEC10A. *Int. J. Mol. Sci.* 21:4818. https://doi.org/10.3390/ijms21144818

Hummelshoj, T., Y.J. Ma, L. Munthe-Fog, T. Bjarnsholt, C. Moser, M.O. Skjoedt, L. Romani, T. Fujita, Y. Endo, and P. Garred. 2012. The interaction pattern of murine serum ficolin-A with microorganisms. *PLoS One*. 7:e38196. https://doi.org/10.1371/journal.pone.0038196

Hyams, C., J. Yuste, K. Bax, E. Camberlein, J.N. Weiser, and J.S. Brown. 2010. *Streptococcus pneumoniae* resistance to complement-mediated immunity is dependent on the capsular serotype. *Infect. Immun.* 78:716–725. https://doi.org/10.1128/IAI.01056-09

Hyams, C., S. Opel, W. Hanage, J. Yuste, K. Bax, B. Henriques-Normark, B.G. Spratt, and J.S. Brown. 2011. Effects of *Streptococcus pneumoniae* strain background on complement resistance. *PLoS One*. 6:e24581. https://doi.org/10.1371/journal.pone.0024581

Hyams, C., K. Trzcinski, E. Camberlein, D.M. Weinberger, S. Chimalapati, M. Noursadeghi, M. Lipsitch, and J.S. Brown. 2013. *Streptococcus pneumoniae* capsular serotype invasiveness correlates with the degree of factor H binding and opsonization with C3b/iC3b. *Infect. Immun.* 81:354–363. https://doi.org/10.1128/IAI.00862-12

Jenne, C.N., and P. Kubes. 2013. Immune surveillance by the liver. *Nat. Immunol.* 14:996–1006. https://doi.org/10.1038/ni.2691

Kang, Y.S., J.Y. Kim, S.A. Bruening, M. Pack, A. Charalambous, A. Pritsker, T.M. Moran, J.M. Loeffler, R.M. Steinman, and C.G. Park. 2004. The C-type lectin SIGN-R1 mediates uptake of the capsular polysaccharide of *Streptococcus pneumoniae* in the marginal zone of mouse spleen. *Proc. Natl. Acad. Sci. USA*. 101:215–220. https://doi.org/10.1073/pnas.0307124101

Kang, Y.S., Y. Do, H.K. Lee, S.H. Park, C. Cheong, R.M. Lynch, J.M. Loeffler, R.M. Steinman, and C.G. Park. 2006. A dominant complement fixation pathway for pneumococcal polysaccharides initiated by SIGN-R1 interacting with C1q. *Cell*. 125:47–58. https://doi.org/10.1016/j.cell.2006.01.046

Kirby, A.C., L. Beattie, A. Maroof, N. van Rooijen, and P.M. Kaye. 2009. SIGNR1-negative red pulp macrophages protect against acute streptococcal sepsis after *Leishmania donovani*-induced loss of marginal zone macrophages. *Am. J. Pathol.* 175:1107–1115. https://doi.org/10.2353/ajpath.2009.090258

Klein, A., M. Zhadkewich, J. Margolick, J. Winkelstein, and G. Bulkley. 1994. Quantitative discrimination of hepatic reticuloendothelial clearance and phagocytic killing. *J. Leukoc. Biol.* 55:248–252. https://doi.org/10.1002/jlb.55.2.248

Kobayashi, S.D., A.R. Porter, B. Freedman, R. Pandey, L. Chen, B.N. Kreiswirth, and F.R. DeLeo. 2018. Antibody-mediated killing of carbapenem-resistant ST258 *Klebsiella pneumoniae* by human neutrophils. *mBio*. 9: e00297-18. https://doi.org/10.1128/mBio.00297-18

Kolaczkowska, E., C.N. Jenne, B.G. Surewaard, A. Thanabalasuriar, W.Y. Lee, M.J. Sanz, K. Mowen, G. Opdenakker, and P. Kubes. 2015. Molecular mechanisms of NET formation and degradation revealed by intravital imaging in the liver vasculature. *Nat. Commun.* 6:6673. https://doi.org/10.1038/ncomms7673

Kolb-Bachofen, V., J. Schlepper-Schafer, W. Vogell, and H. Kolb. 1982. Electron microscopic evidence for an asialoglycoprotein receptor on Kupffer cells: Localization of lectin-mediated endocytosis. *Cell*. 29: 859–866. https://doi.org/10.1016/0092-8674(82)90447-0

Koppel, E.A., C.W. Wieland, V.C. van den Berg, M. Litjens, S. Florquin, Y. van Kooyk, T. van der Poll, and T.B. Geijtenbeek. 2005. Specific ICAM-3 grabbing nonintegrin-related 1 (SIGNR1) expressed by marginal zone macrophages is essential for defense against pulmonary *Streptococcus pneumoniae* infection. *Eur. J. Immunol.* 35:2962–2969. https://doi.org/10.1002/eji.200526216

Krarup, A., U.B. Sorensen, M. Matsushita, J.C. Jensenius, and S. Thiel. 2005. Effect of capsulation of opportunistic pathogenic bacteria on binding of the pattern recognition molecules mannan-binding lectin, L-ficolin, and H-ficolin. *Infect. Immun.* 73:1052–1060. https://doi.org/10.1128/IAI.73.2.1052-1060.2005

Lanoue, A., M.R. Clatworthy, P. Smith, S. Green, M.J. Townsend, H.E. Jolin, K.G. Smith, P.G. Fallon, and A.N. McKenzie. 2004. SIGN-R1 contributes to protection against lethal pneumococcal infection in mice. *J. Exp. Med.* 200:1383–1393. https://doi.org/10.1084/jem.20040795

Lee, W.Y., T.J. Moriarty, C.H. Wong, H. Zhou, R.M. Strieter, N. van Rooijen, G. Chaconas, and P. Kubes. 2010. An intravascular immune response to *Borrelia burgdorferi* involves Kupffer cells and iNKT cells. *Nat. Immunol.* 11:295–302. https://doi.org/10.1038/ni.1855

Lee, C., H.J. Chun, M. Park, R.K. Kim, Y.H. Whang, S.K. Choi, Y.O. Baik, S.S. Park, and I. Lee. 2020. Quality improvement of capsular polysaccharide in *Streptococcus pneumoniae* by purification process optimization. *Front Bioeng. Biotechnol.* 8:39. https://doi.org/10.3389/fbioe.2020.00039

Lepay, D.A., C.F. Nathan, R.M. Steinman, H.W. Murray, and Z.A. Cohn. 1985. Murine Kupffer cells. Mononuclear phagocytes deficient in the generation of reactive oxygen intermediates. *J. Exp. Med.* 161:1079–1096. https://doi.org/10.1084/jem.161.5.1079

Leung, L.S.E., G.J. Szal, and R.H. Drachman. 1972. Increased susceptibility of splenectomized rats to infection with Diplococcus pneumoniae. *J. Infect. Dis.* 126:507–513. https://doi.org/10.1093/infdis/126.5.507

Li, G., F.Z. Hu, X. Yang, Y. Cui, J. Yang, F. Qu, G.F. Gao, and J.R. Zhang. 2012. Complete genome sequence of *Streptococcus pneumoniae* strain ST556, a multidrug-resistant isolate from an otitis media patient. *J. Bacteriol.* 194: 3294–3295. https://doi.org/10.1128/JB.00363-12

Li, P.Z., J.Z. Li, M. Li, J.P. Gong, and K. He. 2014. An efficient method to isolate and culture mouse Kupffer cells. *Immunol. Lett.* 158:52–56. https://doi.org/10.1016/j.imlet.2013.12.002

Li, J., J.W. Li, Z. Feng, J. Wang, H. An, Y. Liu, Y. Wang, K. Wang, X. Zhang, Z. Miao, et al. 2016. Epigenetic switch driven by DNA inversions dictates phase variation in *Streptococcus pneumoniae*. *PLoS Pathog.* 12:e1005762. https://doi.org/10.1371/journal.ppat.1005762

Li, Y., J. Fu, Y. Ling, T. Yago, J.M. McDaniel, J. Song, X. Bai, Y. Kondo, Y. Qin, C. Hoover, et al. 2017. Sialylation on O-glycans protects platelets from clearance by liver Kupffer cells. *Proc. Natl. Acad. Sci. USA.* 114: 8360–8365. https://doi.org/10.1073/pnas.1707662114

Liu, Y., Y. Zeng, Y. Huang, L. Gu, S. Wang, C. Li, D.A. Morrison, H. Deng, and J.R. Zhang. 2019. HtrA-mediated selective degradation of DNA uptake apparatus accelerates termination of pneumococcal transformation. *Mol. Microbiol.* 112:1308–1325. https://doi.org/10.1111/mmi.14364

Lo, S.W., R.A. Gladstone, A.J. van Tonder, J.A. Lees, M. du Plessis, R. Benisty, N. Givon-Lavi, P.A. Hawkins, J.E. Cornick, B. Kwambana-Adams, et al. 2019. Pneumococcal lineages associated with serotype replacement and antibiotic resistance in childhood invasive pneumococcal disease in the post-PCV13 era: An international whole-genome sequencing study. *Lancet Infect. Dis.* 19:759–769. https://doi.org/10.1016/S1473-3099(19)30297-X

Lu, L., Y. Ma, and J.R. Zhang. 2006. *Streptococcus pneumoniae* recruits complement factor H through the amino terminus of CbpA. *J. Biol. Chem.* 281:15464–15474. https://doi.org/10.1074/jbc.M602404200

Mackaness, G.B. 1962. Cellular resistance to infection. *J. Exp. Med.* 116: 381–406. https://doi.org/10.1084/jem.116.3.381

MacParland, S.A., J.C. Liu, X.Z. Ma, B.T. Innes, A.M. Bartczak, B.K. Gage, J. Manuel, N. Khuu, J. Echeverri, I. Linares, et al. 2018. Single cell RNA sequencing of human liver reveals distinct intrahepatic macrophage populations. *Nat. Commun.* 9:4383. https://doi.org/10.1038/s41467-018-06318-7

Martin, S.P., G.P. Kerby, and B.C. Holland. 1949. A method for measuring removal of bacteria from the blood by the various organs of the intact animal. *P Soc. Exp. Biol. Med.* 72:63–68. https://doi.org/10.3181/00379727-72-17333

Mavroidi, A., D. Godoy, D.M. Aanensen, D.A. Robinson, S.K. Hollingshead, and B.G. Spratt. 2004. Evolutionary genetics of the capsular locus of serogroup 6 pneumococci. *J. Bacteriol.* 186:8181–8192. https://doi.org/10.1128/JB.186.24.8181-8192.2004

McGreal, E.P., M. Rosas, G.D. Brown, S. Zamze, S.Y.C. Wong, S. Gordon, L. Martinez-Pomares, and P.R. Taylor. 2006. The carbohydrate-recognition domain of Dectin-2 is a C-type lectin with specificity for high mannose. *Glycobiology*. 16:422–430. https://doi.org/10.1093/glycob/cwj077

Medzhitov, R. 2007. Recognition of microorganisms and activation of the immune response. *Nature*. 449:819–826. https://doi.org/10.1038/nature06246

Monroe, R.S., and B.E. Huber. 1994. The major form of the murine asialoglycoprotein receptor: cDNA sequence and expression in liver, testis and epididymis. *Gene*. 148:237–244. https://doi.org/10.1016/0378-1119(94)90694-7

Moradali, M.F., and B.H.A. Rehm. 2020. Bacterial biopolymers: From pathogenesis to advanced materials. *Nat. Rev. Microbiol.* 18:195–210. https://doi.org/10.1038/s41579-019-0313-3

Munford, R.S., and A.F. Suffredini. 2014. Sepsis, severe sepsis and septic shock. In Mandell, Douglas, and Bennett's Principles and Practice of Infectious Diseases. J.E. Bennett, R.D. Dolin, and M.J. Blaser, editors. Elsevier Health Sciences, Philadelphia. 914–934

Musher, D.M., and A.R. Thorner. 2014. Community-acquired pneumonia. *N. Engl. J. Med.* 371:1619–1628. https://doi.org/10.1056/NEJMra1312885

Nahm, M.H., and J. Katz. 2012. Immunity to extracellular bacteria. In Fundamental Immunology. W.E. Paul, editor. Lippincott-Raven Publishers, Philadephia. 1001–1015

Pai, R., R.E. Gertz, and B. Beall. 2006. Sequential multiplex PCR approach for determining capsular serotypes of *Streptococcus pneumoniae* isolates. *J. Clin. Microbiol.* 44:124–131. https://doi.org/10.1128/JCM.44.1.124-131.2006

Pangburn, M.K., and H.J. Muller-Eberhard. 1978. Complement C3 convertase: Cell surface restriction of beta1H control and generation of restriction on neuraminidase-treated cells. *Proc. Natl. Acad. Sci. USA.* 75:2416–2420. https://doi.org/10.1073/pnas.75.5.2416

Paton, J.C., and C. Trappetti. 2019. *Streptococcus pneumoniae* capsular polysaccharide. *Microbiol. Spectr.* 7. https://doi.org/10.1128/microbiolspec.GPP3-0019-2018

Pertics, B.Z., A. Cox, A. Nyul, N. Szamek, T. Kovacs, and G. Schneider. 2021. Isolation and characterization of a novel lytic bacteriophage against the K2 capsule-expressing hypervirulent *Klebsiella pneumoniae* strain 52145, and identification of its functional depolymerase. *Microorganisms*. 9: 650. https://doi.org/10.3390/microorganisms9030650

Robbins, J.B., G.H. McCracken Jr., E.C. Gotschlich, F. Orskov, I. Orskov, and L.A. Hanson. 1974. *Escherichia coli* K1 capsular polysaccharide associated with neonatal meningitis. *N. Engl. J. Med.* 290:1216–1220. https://doi.org/10.1056/NEJM197405302902202

Rogers, D.E. 1956. Studies on bacteriemia. I. Mechanisms relating to the persistence of bacteriemia in rabbits following the intravenous injection of staphylococci. *J. Exp. Med.* 103:713–742. https://doi.org/10.1084/jem.103.6.713

Rudd, K.E., S.C. Johnson, K.M. Agesa, K.A. Shackelford, D. Tsoi, D.R. Kievlan, D.V. Colombara, K.S. Ikuta, N. Kissoon, S. Finfer, et al. 2020. Global, regional, and national sepsis incidence and mortality, 1990–2017: Analysis for the global burden of disease study. *Lancet*. 395:200–211. https://doi.org/10.1016/S0140-6736(19)32989-7

Schlottmann, S.A., N. Jain, N. Chirmule, and M.T. Esser. 2006. A novel chemistry for conjugating pneumococcal polysaccharides to Luminex microspheres. *J. Immunol. Methods*. 309:75–85. https://doi.org/10.1016/j.jim.2005.11.019

Scott, C.L., F. Zheng, P. De Baetselier, L. Martens, Y. Saeys, S. De Prijck, S. Lippens, C. Abels, S. Schoonooghe, G. Raes, et al. 2016. Bone marrow-derived monocytes give rise to self-renewing and fully differentiated Kupffer cells. *Nat. Commun.* 7:10321. https://doi.org/10.1038/ncomms10321

Shia, M.A., and H.F. Lodish. 1989. The two subunits of the human asialoglycoprotein receptor have different fates when expressed alone in fibroblasts. *Proc. Natl. Acad. Sci. USA*. 86:1158–1162. https://doi.org/10.1073/pnas.86.4.1158

Shinefield, H.R., C.R. Steinberg, and D. Kaye. 1966. Effect of splenectomy on the susceptibility of mice inoculated with Diplococcus pneumoniae. *J. Exp. Med.* 123:777–794. https://doi.org/10.1084/jem.123.5.777

Sjostrom, K., C. Spindler, A. Ortqvist, M. Kalin, A. Sandgren, S. Kuhlmann-Berenzon, and B. Henriques-Normark. 2006. Clonal and capsular types decide whether pneumococci will act as a primary or opportunistic pathogen. *Clin. Infect. Dis.* 42:451–459. https://doi.org/10.1086/499242

Sorensen, A.L., V. Rumjantseva, S. Nayeb-Hashemi, H. Clausen, J.H. Hartwig, H.H. Wandall, and K.M. Hoffmeister. 2009. Role of sialic acid for platelet life span: Exposure of beta-galactose results in the rapid clearance of platelets from the circulation by asialoglycoprotein receptor-expressing liver macrophages and hepatocytes. *Blood*. 114: 1645–1654. https://doi.org/10.1182/blood-2009-01-199414

Stockert, R.J. 1995. The asialoglycoprotein receptor: Relationships between structure, function, and expression. *Physiol. Rev.* 75:591–609. https://doi.org/10.1152/physrev.1995.75.3.591

Subramanian, K., D.R. Neill, H.A. Malak, L. Spelmink, S. Khandaker, G. Dalla Libera Marchiori, E. Dearing, A. Kirby, M. Yang, A. Achour, et al. 2019. Pneumolysin binds to the mannose receptor C type 1 (MRC-1) leading to anti-inflammatory responses and enhanced pneumococcal survival. *Nat. Microbiol.* 4:62–70. https://doi.org/10.1038/s41564-018-0280-x

Sun, D., P. Sun, H. Li, M. Zhang, G. Liu, A.B. Strickland, Y. Chen, Y. Fu, J. Xu, M. Yosri, et al. 2019. Fungal dissemination is limited by liver macrophage filtration of the blood. *Nat. Commun.* 10:4566. https://doi.org/10.1038/s41467-019-12381-5

Sung, C.K., H. Li, J.P. Claverys, and D.A. Morrison. 2001. An rpsL cassette, janus, for gene replacement through negative selection in *Streptococcus pneumoniae*. *Appl. Environ. Microb.* 67:5190–5196. https://doi.org/10.1128/AEM.67.11.5190-5196.2001

Surewaard, B.G., J.F. Deniset, F.J. Zemp, M. Amrein, M. Otto, J. Conly, A. Omri, R.M. Yates, and P. Kubes. 2016. Identification and treatment of

the *Staphylococcus aureus* reservoir in vivo. *J. Exp. Med.* 213:1141–1151. https://doi.org/10.1084/jem.20160334

Tabula Muris Consortium. 2018. Single-cell transcriptomics of 20 mouse organs creates a Tabula Muris. *Nature*. 562:367–372. https://doi.org/10.1038/s41586-018-0590-4

Taylor, C., and I.S. Roberts. 2002. The regulation of capsule expression. *In* Bacterial Adhesion to Host Tissues- Mechanisms and Consequences. M. Wilson, editor. Cambridge University Press, Cambridge. 115–138

Theilacker, C., K. Ludewig, A. Serr, J. Schimpf, J. Held, M. Bogelein, V. Bahr, S. Rusch, A. Pohl, K. Kogelmann, et al. 2016. Overwhelming post-splenectomy infection: A prospective multicenter cohort study. *Clin. Infect. Dis.* 62:871–878. https://doi.org/10.1093/cid/civ1195

Troy, F.A., 2nd. 1992. Polysialylation: From bacteria to brains. *Glycobiology*. 2: 5–23. https://doi.org/10.1093/glycob/2.1.5

Trzcinski, K., C.M. Thompson, and M. Lipsitch. 2003. Construction of otherwise isogenic serotype 6B, 7F, 14, and 19F capsular variants of *Streptococcus pneumoniae* strain TIGR4. *Appl. Environ. Microbiol.* 69:7364–7370. https://doi.org/10.1128/AEM.69.12.7364-7370.2003

Wang, J., and P. Kubes. 2016. A reservoir of mature cavity macrophages that can rapidly invade visceral organs to affect tissue repair. *Cell*. 165: 668–678. https://doi.org/10.1016/j.cell.2016.03.009

Wang, Y., S. Wang, W. Chen, L. Song, Y. Zhang, Z. Shen, F. Yu, M. Li, and Q. Ji. 2018a. CRISPR-Cas9 and CRISPR-assisted cytidine deaminase enable precise and efficient genome editing in *Klebsiella pneumoniae*. *Appl. Environ. Microbiol.* 84:e01834–18. https://doi.org/10.1128/AEM.01834-18

Wang, Y., Z. Wen, X. Pan, D.E. Briles, Y. He, and J.R. Zhang. 2018b. Novel immunoprotective proteins of *Streptococcus pneumoniae* identified by opsonophagocytosis killing screen. *Infect. Immun.* 86:e00423-18. https://doi.org/10.1128/IAI.00423-18

Weinberger, D.M., Z.B. Harboe, E.A. Sanders, M. Ndiritu, K.P. Klugman, S. Ruckinger, R. Dagan, R. Adegbola, F. Cutts, H.L. Johnson, et al. 2010. Association of serotype with risk of death due to pneumococcal pneumonia: A meta-analysis. *Clin. Infect. Dis.* 51:692–699. https://doi.org/10.1086/655828

Wen, Z., and J.-R. Zhang. 2015. Bacterial capsules. *In* Molecular Medical Microbiology. Y.-W. Tang, M. Sussman, D. Liu, I. Poxton, and J. Schwartzman, editors. Academic Press, Amsterdam. 33–52

Wen, Z., Y. Liu, F. Qu, and J.R. Zhang. 2016. Allelic variation of the capsule promoter diversifies encapsulation and virulence in *Streptococcus pneumoniae*. *Sci Rep.* 6:30176. https://doi.org/10.1038/srep30176

Wessels, M.R. 2006. Capsular polysaccharide of group A streptococci. *In* Gram-Positive Pathogens. V.A. Fischetti, R.P. Novick, J.J. Ferretti, D.A. Portnoy, and J.I. Rood, editors. ASM Press, Washington, D.C. 37–46

Whitaker, A.N. 1968. The effect of previous splenectomy on the course of pneumococcal bacteremia in mice. *J. Pathol. Bacteriol.* 95:357–376. https://doi.org/10.1002/path.1700950203

White, B. 1938. Pathogenicity of pneumococcus: Man. *In* The Biology of Pneumococcus. Harvard University Press, Cambridge, MA. 214–237

Whitfield, C., S.S. Wear, and C. Sande. 2020. Assembly of bacterial capsular polysaccharides and exopolysaccharides. *Annu. Rev. Microbiol.* 74: 521–543. https://doi.org/10.1146/annurev-micro-011420-075607

Wilkinson, B.J., P.K. Peterson, and P.G. Quie. 1979. Cryptic peptidoglycan and the antiphagocytic effect of the *Staphylococcus aureus* capsule: Model for the antiphagocytic effect of bacterial cell surface polymers. *Infect. Immun.* 23:502–508. https://doi.org/10.1128/iai.23.2.502-508.1979

Wong, C.H., C.N. Jenne, B. Petri, N.L. Chrobok, and P. Kubes. 2013. Nucleation of platelets with blood-borne pathogens on Kupffer cells precedes other innate immunity and contributes to bacterial clearance. *Nat. Immunol.* 14:785–792. https://doi.org/10.1038/ni.2631

Wright, S.D., and M.T. Jong. 1986. Adhesion-promoting receptors on human macrophages recognize *Escherichia coli* by binding to lipopolysaccharide. *J. Exp. Med.* 164:1876–1888. https://doi.org/10.1084/jem.164.6.1876

Xiong, H., R.A. Carter, I.M. Leiner, Y.W. Tang, L. Chen, B.N. Kreiswirth, and E.G. Pamer. 2015. Distinct Contributions of neutrophils and CCR2$^+$ monocytes to pulmonary clearance of different *Klebsiella pneumoniae* strains. *Infect. Immun.* 83:3418–3427. https://doi.org/10.1128/IAI.00678-15

Zamze, S., L. Martinez-Pomares, H. Jones, P.R. Taylor, R.J. Stillion, S. Gordon, and S.Y. Wong. 2002. Recognition of bacterial capsular polysaccharides and lipopolysaccharides by the macrophage mannose receptor. *J. Biol. Chem.* 277:41613–41623. https://doi.org/10.1074/jbc.M207057200

Zeng, Z.T., B.G.J. Surewaard, C.H.Y. Wong, J.A. Geoghegan, C.N. Jenne, and P. Kubes. 2016. CRIg functions as a macrophage pattern recognition receptor to directly bind and capture blood-borne Gram-positive bacteria. *Cell Host Microbe*. 20:99–106. https://doi.org/10.1016/j.chom.2016.06.002

Zhang, J.R., K.E. Mostov, M.E. Lamm, M. Nanno, S. Shimida, M. Ohwaki, and E. Tuomanen. 2000. The polymeric immunoglobulin receptor translocates pneumococci across human nasopharyngeal epithelial cells. *Cell*. 102:827–837. https://doi.org/10.1016/s0092-8674(00)00071-4

Zhang, M., L. Liu, X. Lin, Y. Wang, Y. Li, Q. Guo, S. Li, Y. Sun, X. Tao, D. Zhang, et al. 2020. A translocation pathway for vesicle-mediated unconventional protein secretion. *Cell*. 181:637–652.e15. https://doi.org/10.1016/j.cell.2020.03.031

Supplemental material

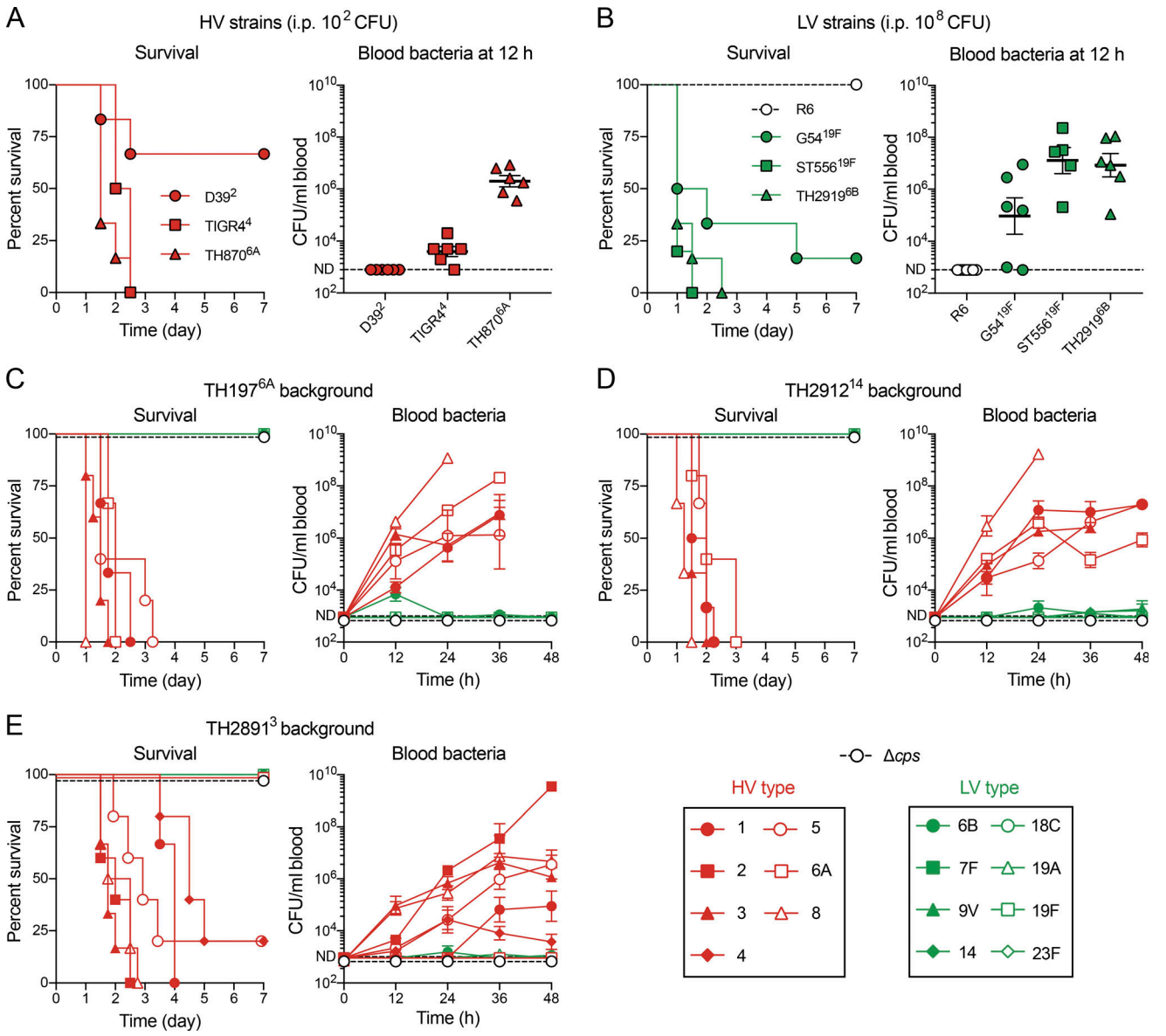

Figure S1. **Serotype-related variations in the virulence level of *S. pneumoniae*. (A)** Survival (left) and bacteremia levels (right) of mice inoculated i.p. with 10^2 CFU of representative HV (D39, TIGR4, and TH870) strains. n = 5–7. **(B)** Survival (left) and bacteremia levels (right) of mice inoculated i.p. with 10^8 CFU of unencapsulated R6 and representative LV (G54, ST556, and TH2919) strains. n = 5–7. **(C–E)** Survival (left) and bacteremia (right) levels of mice were assessed by i.p. infection with 10^4 CFU of the isogenic capsule variants generated in serotype 6A strain TH197 (C), serotype 14 strain TH2912 (D), and serotype 3 strain TH2891 (E). n = 5–6. All mice were used on a CD1 background. Data were pooled from two independent experiments.

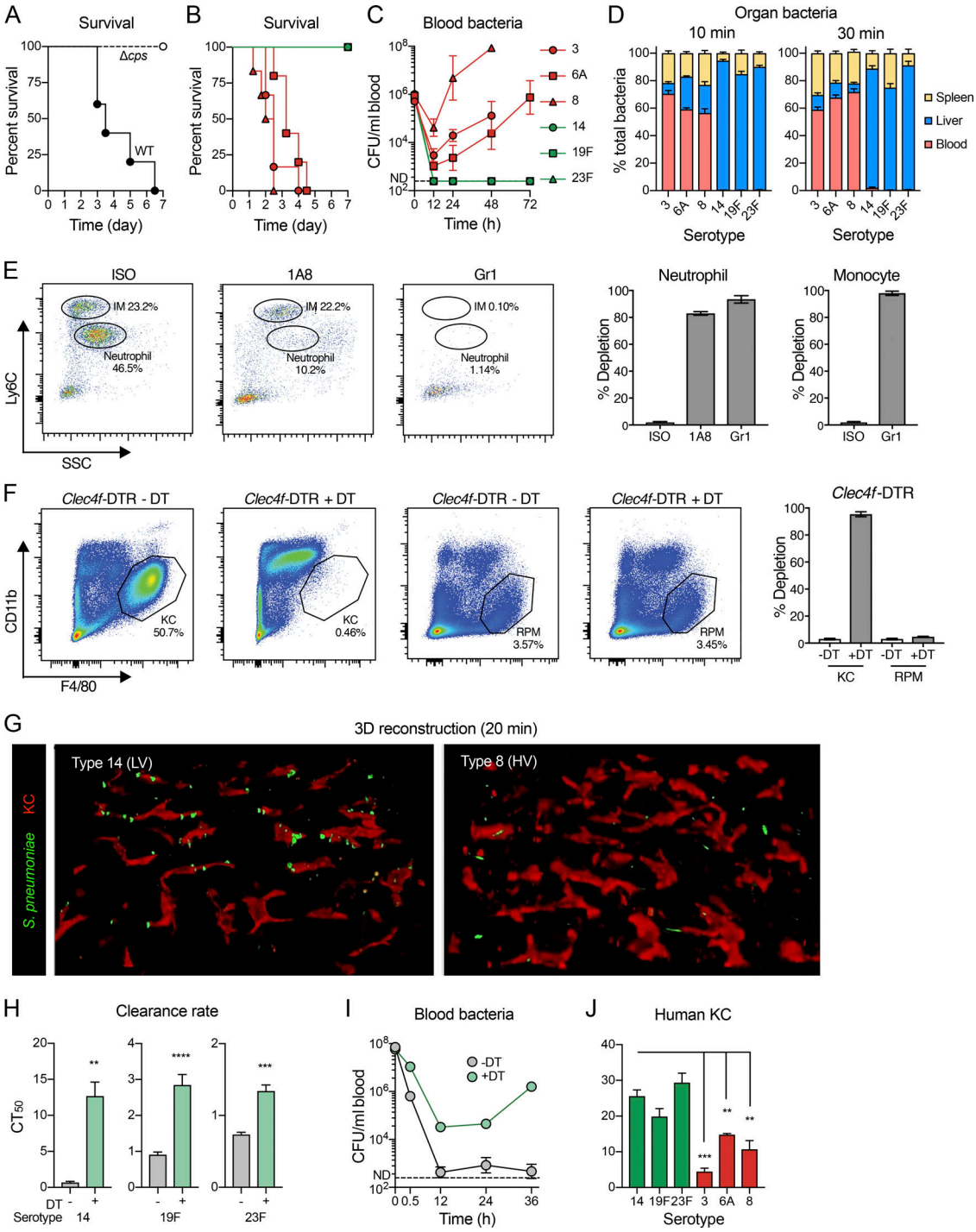

Figure S2. **Capsule-related capture of pneumococci by liver KCs. (A and B)** Survival of mice after i.v. infection with 10^6 CFU of WT TH870 and acapsular mutant (A) or isogenic capsule-switched derivatives (B). *n* = 5–6. **(C)** Bacteremia kinetics in the mice during the first 72 h after i.v. infection. *n* = 5–6. **(D)** Proportional distribution of isogenic HV and LV pneumococci in blood, liver, and spleen 10 and 30 min after infection. *n* = 3. **(E)** Depletion efficiency of neutrophil and monocyte verified by flow cytometry. Mice were treated with 500 µg anti-Ly6G (1A8), 500 µg anti-Ly6C/Ly6G (Gr1), or the isotype controls (ISO). The ratios of neutrophils ($Ly6C^{low}/SSC^{high}$) and inflammatory monocytes ($Ly6C^{high}/SSC^{low}$) in the blood were measured in the myeloid populations ($CD45^+/CD11b^+$). *n* = 3. **(F)** Depletion efficiency of tissue-resident macrophage verified by flow cytometry. The *Clec4f*-DTR mice were treated with 10 ng/g DT. The populations of liver KC and spleen red pulp macrophage (RPM) were measured 24 h after DT treatment. Depletion efficiency was calculated by comparing the ratios of macrophages ($CD11b^{low}/F4/80^+$) in the immune cells ($CD45^+$). *n* = 3. **(G)** 3D rendering of the liver sinusoid revealing bacterium-binding KCs 20 min after inoculation. **(H)** Clearance rates of LV isogenic derivatives of TH870 (type 14, 19F, and 23F) during the first 30 min after infection with 10^6 CFU in *Clec4f*-DTR mice treated with (+) or without (–) DT. *n* = 5–10. **(I)** Sustained bacteremia levels of LV strain $TH870^{14}$ in the KC-depleted mice after i.v. infection with 10^8 CFU. *n* = 5. **(J)** In vitro binding of pneumococcal isogenic capsule variants to primary human KCs. *n* = 3. Mice were used on CD1 (A–D) or C57BL/6 (E–I) backgrounds. Data are representative results (D–G and J) or pooled (A–C, H, and I) from two independent experiments. Two-way ANOVA with Sidak's multiple comparisons test (H), ordinary one-way ANOVA with Tukey's multiple comparisons test (J), **, P < 0.01, ***, P < 0.001, ****, P < 0.0001.

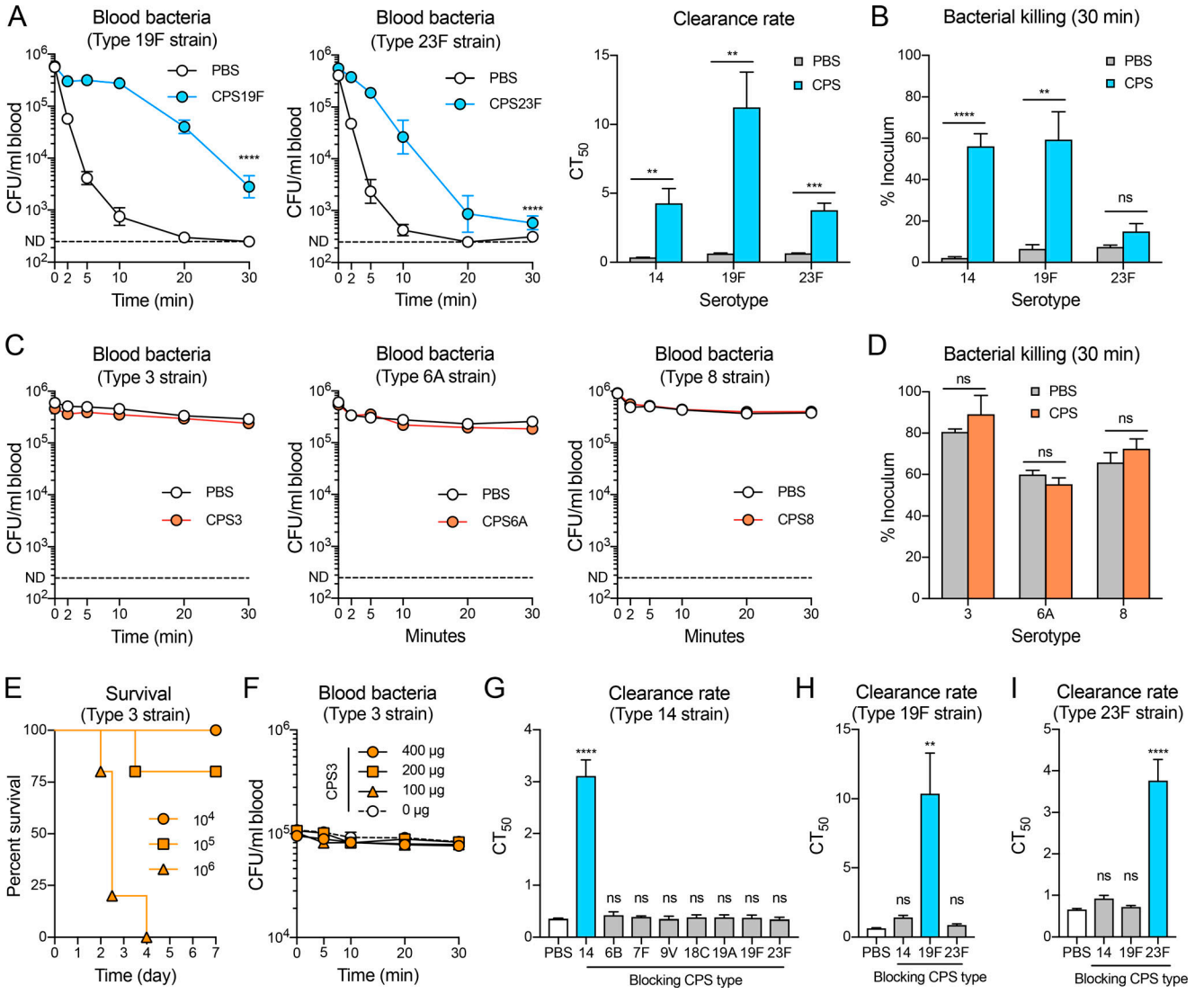

Figure S3. **Serotype-specific inhibition of bacterial clearance by free CPSs. (A)** Blocking effect of free CPS19F and CPS23F on the clearance of homologous serotypes of pneumococci were assessed as in Fig. 7 B. *n* = 6. **(B)** Impact of free LV CPSs on elimination of homologous serotypes of pneumococci during the first 30 min of infection. *n* = 3–6. **(C)** Impact of free CPS3, CPS6A, and CPS8 on the clearance of homologous serotype derivatives of TH870 was assessed as in A. *n* = 3–6. **(D)** Same as B except using HV CPSs. *n* = 3–6. **(E)** Survival of mice infected i.v. with 10^4–10^6 CFU of serotype-3 pneumococci. *n* = 5. **(F)** Impact of CPS3 on the clearance of sublethal dose (10^5 CFU) of serotype-3 pneumococci during the first 30 min of infection. *n* = 3. **(G)** Clearance rates of serotype-14 pneumococci in mice pretreated with one of the eight free CPSs (400 µg/mouse) before i.v. infection with 10^6 CFU. *n* = 3–6. **(H)** Clearance rates of serotype-19F pneumococci in mice pretreated with each type of free CPSs (400 µg/mouse) before i.v. infection with 10^6 CFU. *n* = 3–6. **(I)** Same as H except using serotype-23F pneumococci as an inoculum. *n* = 3–6. All mice were used on a CD1 background. Data were pooled from two independent experiments, except F (one experiment). Two-way ANOVA with Tukey's (A, left and middle panels) and Sidak's (A, right panel, B, and D) multiple comparisons test, Ordinary one-way ANOVA with Tukey's multiple comparisons test (G–I), **, P < 0.01, ***, P < 0.001, ****, P < 0.0001.

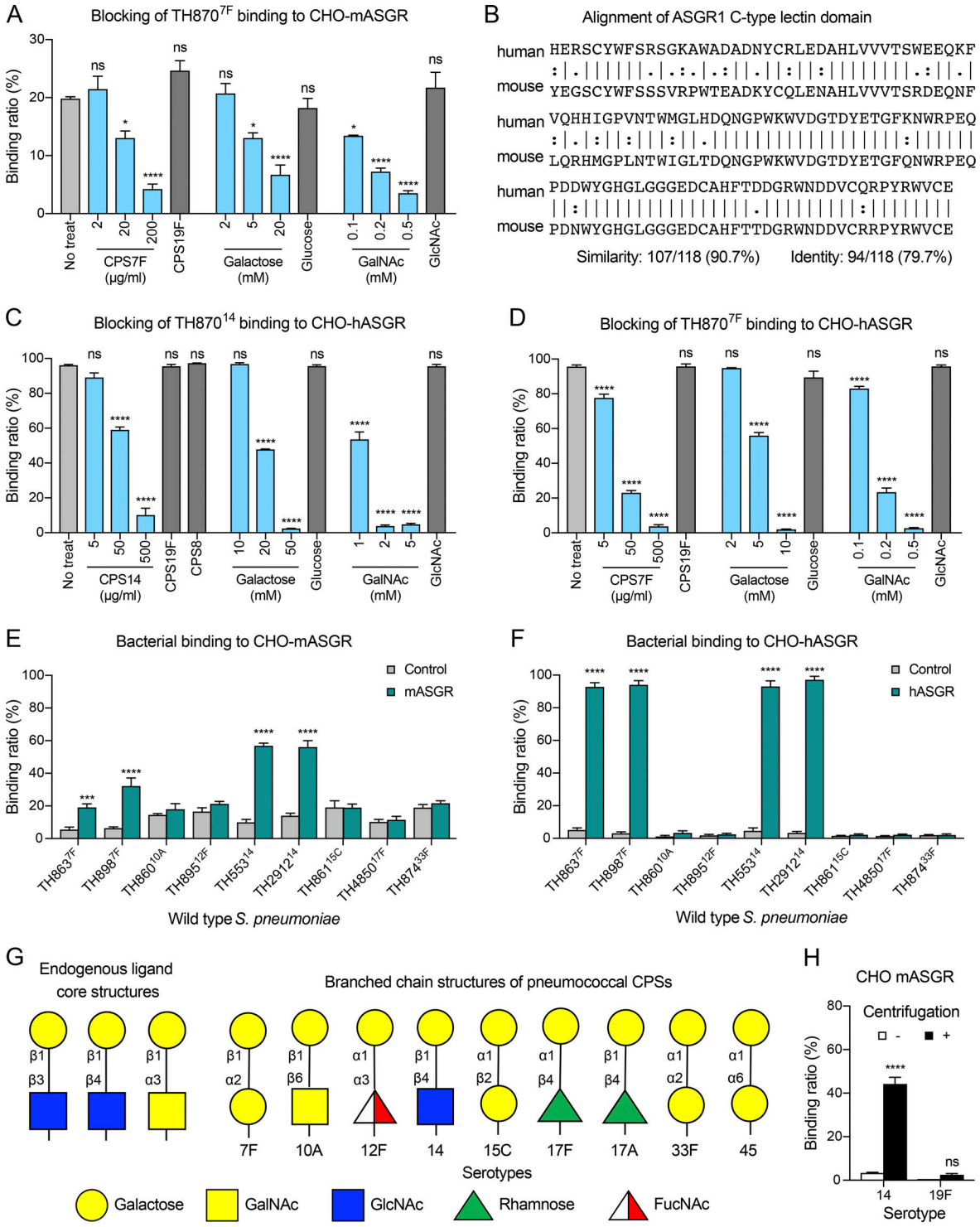

Figure S4. **ASGR-mediated KC capture of serotype-7F and -14 pneumococci. (A)** Dose-dependent blocking of mASGR-mediated TH870^{7F} adherence by free CPS7F, galactose, or GalNAc. *n* = 3. **(B)** Alignment of the C-type lectin domains of human and mouse ASGR1. **(C)** Same as A except using hASGR-transfected CHO cells and serotype-14 pneumococci. *n* = 3. **(D)** Same as C except using serotype-7F pneumococci. *n* = 3. **(E)** Impact of mASGR on adherence to CHO cells by natural pneumococcal strains with terminal galactose in the CPSs. Bacterial adherence was quantified as in Fig. 7 D. *n* = 3. **(F)** Same as E except using hASGR-transfected cells. *n* = 3. **(G)** The disaccharide structures of endogenous ASGR ligands and the known terminal galactose-containing capsules in *S. pneumoniae*. Only CPS14 has the identical signature with the native ligand core structure Galβ1,4GlcNAc. **(H)** Effect of centrifugation on receptor-mediated bacterial adhesion to host cells. Isogenic serotype-14 or -19F pneumococci were suspended in F-12K medium to a density of 10^6 CFU/ml; 50 μl of bacterial suspension was added to the monolayers of ASGR-expressing CHO cells in 96-well plates; mild centrifugation (500 *g* for 5 min) was applied immediately after bacterial suspensions were added to cell monolayers to mimic the sheer force that blood-borne bacteria experience in the blood circulation. *n* = 3. All data were representative results from two to three independent experiments. Ordinary one-way ANOVA with Tukey's multiple comparisons test (A, C, and D), two-way ANOVA with Sidak's multiple comparisons test (E, F, and H), *, P < 0.05, ***, P < 0.001, ****, P < 0.0001.

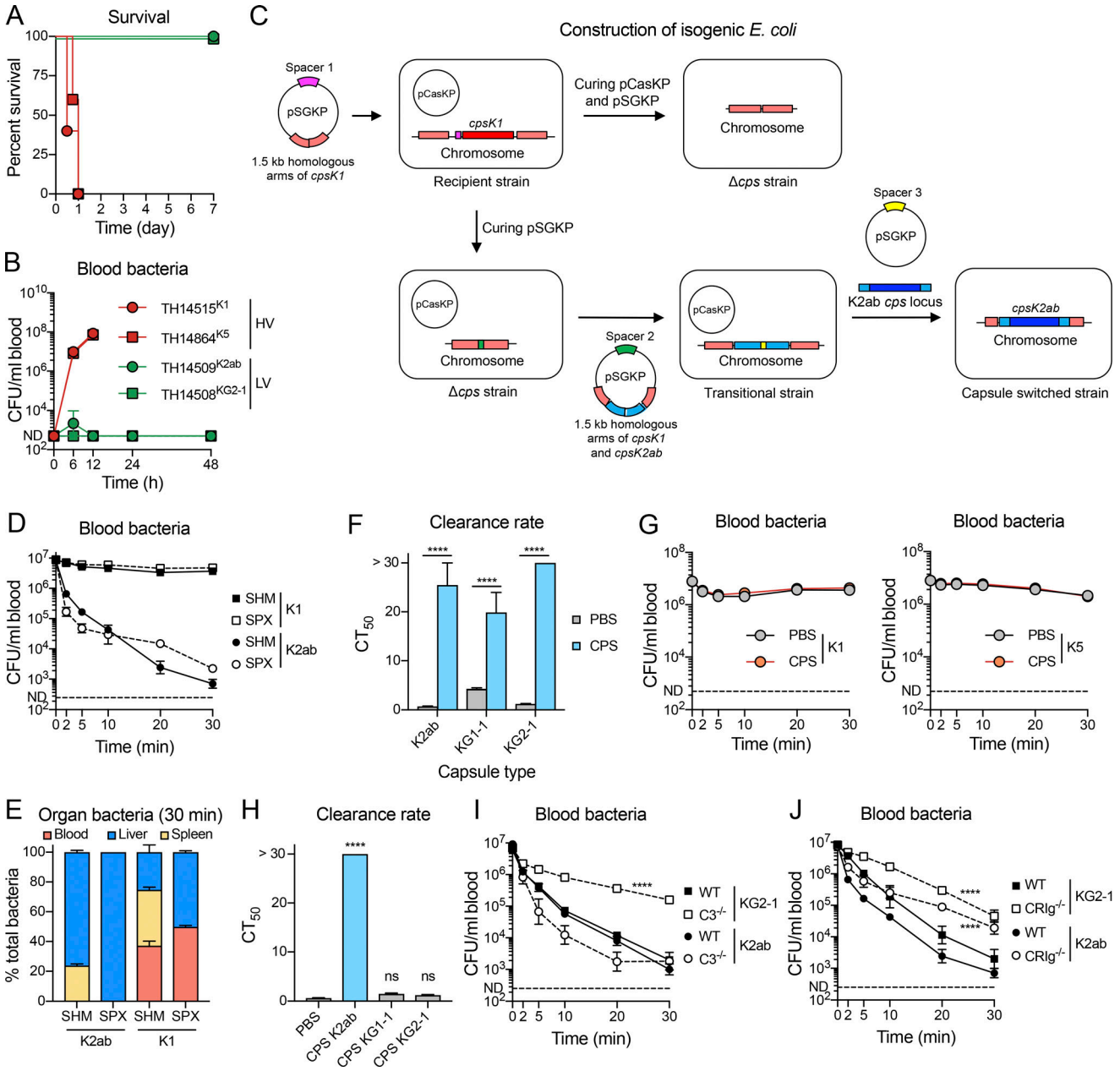

Figure S5. **Capsule type–dependent evasion of hepatic clearance of invasive *E. coli*. (A and B)** Survival (A) and bacteremia (B) levels of mice infected i.p. with 10^7 CFU of representative HV (red line) and LV (green line) invasive *E. coli* isolates. Capsular type of each strain is denoted with superscript characters. $n = 5$. **(C)** Schematic illustration of the experimental procedures for genetic switching of the *cps* genes in *E. coli*. The original *cps* locus of the host strain was deleted by Cas9-mediated genome editing with the *cps* gene-targeting guide RNA, followed by DNA repair through homologous recombination with the 1.5 kb up- and downstream arms of the *cps* locus. The recipient *cps* genes were introduced into the *cps*-negative host mutant through another cycle of Cas9-mediated genome editing and repair. See Materials and methods for more details. **(D and E)** Bacteremia kinetics (D) and proportional distribution (E) of isogenic *E. coli* strains in SPX mice during the first 30 min after infection. $n = 3$. **(F)** Clearance rates of LV *E. coli* strains in the presence of free homologous CPSs (400 µg) before i.v. infection with 10^7 CFU. $n = 3$–5. **(G)** Bacteremia kinetics of HV K1 (left) and K5 (right) *E. coli* in the presence of corresponding CPSs during the first 30 min after infection. $n = 3$. **(H)** Clearance rates of LV K2ab *E. coli* in mice pretreated with each type of free CPSs (400 µg) before i.v. infection with 10^7 CFU. $n = 3$–5. **(I and J)** Bacteremia kinetics of LV isogenic *E. coli* in $C3^{-/-}$ (I) and $CRIg^{-/-}$ (J) mice during the first 30 min after infection. $n = 3$. All mice were used in C57BL/6 background. Data were from one experiment (D, E, G, I, and J) or pooled (A, B, F, and H) from two independent experiments. Two-way ANOVA with Sidak's (F) or Tukey's (I and J) multiple comparisons test, Ordinary one-way ANOVA with Tukey's multiple comparisons test (H), ****, $P < 0.0001$.

Video 1. **KC capture of unencapsulated but not WT *S. pneumoniae*.** Bacteria were labeled with FITC (green) and inoculated i.v. at 5×10^7 CFU for real-time visualization in the first 5 min. KCs and liver sinusoid vasculatures were stained with AF647 anti-F4/80 (red) and AF594 anti-CD31 (cyan), respectively. The Δ*cps* bacteria were rapidly captured by KCs, while the WT isogenic counterparts kept moving in the blood. Graphic analysis was shown in Fig. 5 F. The video is 30 frames per second.

Video 2. **Diminished liver capture of Δ*cps* in KC-deficient mice.** Pneumococcal capture was monitored in the first 5 min after inoculation with 5×10^7 CFU in *Clec4f*-DTR mice treated with (+DT) or without 10 ng/g DT (–DT). Specific depletion of KCs abolished the capture of the Δ*cps* in the liver sinusoids. Graphic analysis was shown in Fig. 5 G. The video is 30 frames per second.

Video 3. **KC capture of LV type 14 but not HV type 8 *S. pneumoniae*.** Bacteria were labeled with FITC (green) and inoculated i.v. at 5×10^7 CFU for real-time visualization in the first 2 min. KCs and vasculature were stained with AF647 anti-F4/80 (red) and AF594 anti-CD31 (cyan), respectively. Graphic analysis was shown in Fig. 6 A. The video is 30 frames per second.

Video 4. **Diminished liver capture of type 14 *S. pneumoniae* in KC-deficient mice.** Pneumococcal capture was monitored in the first 2.5 min after inoculation with 5×10^7 CFU in *Clec4f*-DTR mice treated with or without DT. Graphic analysis was shown in Fig. 6 B. The video is 30 frames per second.

Video 5. **Inhibition of free CPS14 to KC capture of type 14 *S. pneumoniae*.** Pneumococcal capture was monitored in the first 4 min after inoculation with 5×10^7 CFU in mice treated with or without 400 µg CPS14. Graphic analysis was shown in Fig. 7 F. The video is 30 frames per second.

Video 6. **KC capture of LV type K2ab but not HV type K1 *E. coli*.** The same with Video 3 except of using isogenic *E. coli* strains. Graphic analysis was shown in Fig. 9 F. The video is 30 frames per second.

Video 7. **Inhibition of free CPS K2ab to KC capture of type K2ab *E. coli*.** The same with Video 5 except of using type K2ab *E. coli*. Graphic analysis was shown in Fig. 9 K. The video is 30 frames per second.

Provided online are Table S1, Table S2, and Table S3. Table S1 summarizes the virulence phenotypes of *S. pneumoniae* and *E. coli* clinical isolates. Table S2 shows the screening result of CPS14-binding proteins by mass spectrometry. Table S3 summarizes bacterial strains, plasmids, primers, and mutagenesis procedures in this study.